INSTITUTE
FOR
AEROSPACE STUDIES

UNIVERSITY OF TORONTO

AERODYNAMIC INTERFERENCE OF HIGH SPEED GROUND VEHICLES

by

G. W. Johnston, B. V. Seshagiri and N. D. Ellis

June 1976

UTIAS Report No. 185
CN ISSN 0082-5255

AERODYNAMIC INTERFERENCE OF HIGH SPEED GROUND VEHICLES

by

G. W. Johnston, B. V. Seshagiri and N. D. Ellis

Submitted June 1974

June 1976

UTIAS Report 185
CN ISSN 0082-5255

Acknowledgement

The authors would like to acknowledge the assistance of Dr. A. Palm-Leis of the Urban Systems Research Department of the Ontario Ministry of Transportation and Communications in carrying out this investigation. Dr. Palm-Leis identified the problem area and provided valuable guidance during the course of the actual study program. The generous support of the above Ministry in providing necessary contract funding is also gratefully acknowledged.

Summary

A two-dimensional, incompressible, potential flow solution based on A.M.O. Smith's method has been developed capable of predicting the unsteady interference pressure loadings on either moving or stationary bodies of arbitrary shape due to the passage of a second body. The pressure distribution has been suitably integrated to yield overall forces (side and axial) and moments (rolling and yawing). Effects of crosswinds of arbitrary magnitude and direction can be accurately included. The results of a wide range of computations using different body configurations are presented and analysed.

The studies carried out indicate that substantial aerodynamic interference loads may be expected under real train passage conditions. These loads, impulsive in nature, depend on the type of body geometry, the lateral spacing between the bodies, and the closing velocity. In general, streamlining greatly reduces these loads, as does increased lateral spacing. Crosswinds significantly alter the predicted loadings, tending to increase them. The interference loading induced on a stationary vehicle when passed by a moving vehicle appears to impose the most critical design loads, for conditions of zero crosswind.

Velocity scaling of the interference loadings presents inherent difficulties due to the basic unsteady nature of the problem. No simple and generally applicable velocity scaling laws are expected to emerge for this problem, however, over limited ranges of conditions "ad hoc" velocity rules (trends) can certainly be obtained. The basic unsteady nature of this problem also greatly complicates experimental studies. The usual steady state wind tunnel methods will generally be inadequate; preference is strongly indicated for true unsteady motion simulation at reduced physical scale.

TABLE OF CONTENTS

1. LITERATURE REVIEW

A fairly large body of literature has grown up during the past decade concerning the aerodynamic problems of high speed trains. Most of it concerns three broad areas:

(1) The drag of high speed trains.

(2) Problems of high speed trains entering and passing through tunnels.

(3) Problems due to the pressure wave set up when a high speed train passes either a stationary train or another train moving in the opposite direction, in free space.

The present review is concerned with the last type of problem only. The problem can be attributed to the pressure which develops around the body due to the motion of the body. The magnitude and direction of the net pressure field is a function of the shape of the body and the speed of travel. Consequently when a high speed train passes either a stationary train or another train passing in the opposite direction, the pressure fields can impose large fluctuating loads on the trains. In this report the pressure pulses will be categorized into two types:

(1) The "cab" pulse.

(2) The "coach" pulse.

The cab pulse is measured at the front of the measuring train as the passing train goes by. The coach pulse is measured somewhere further to the rear of the measuring train. Both theoretical and experimental work has been done in an attempt to predict the magnitude and duration of the pressure pulse.

1(a) Review of Theoretical Methods

All the theoretical approaches are based on potential flow theory. They can be categorized into two distinct methods. The first method utilizes the concept of singularities and their images to satisfy Laplace's equation and the appropriate boundary conditions and thus arrive at a solution to the flow field for a body (or bodies) moving in an incompressible, inviscid, irrotational fluid.

Carpenter (Ref. 1) gave a solution to the problem of 2 cylinders moving in an infinite fluid. The cylinders with their generators perpendicular to the plane of motion are moving with arbitrary translational velocities. The cylinders are replaced by moving doublets. Each of the doublets have their respective images in the other cylinder yielding an infinity of doublets together with their images. The complex potential due to the entire system is given. For purposes of computation, Carpenter suggests that just the first few terms (three) are usually sufficient. He also gives correction factors to account for the dropped terms. He extends the solution to the case of any number of moving cylinders and gives examples of several flow situations using the above methods.

Kawaguti (Ref. 2) has adopted an identical approach. He considers two-dimensional cylinders as well as spheres. He restricts his calculations to the case of two bodies moving with their axes parallel to each other, but in opposite directions with different velocities. Whereas the image of a doublet in a sphere is a continuous distribution of doublets starting from the centre of the sphere up to the inverse point. This complicates the calculations considerably for the sphere cases. Kawaguti has extended his solutions to calculate the pressure variation using the unsteady Bernoulli's equation.

Pukuchi (Ref. 3) has attempted to solve the problem in a slightly different manner. Instead of doublets, he places a moving source, and considers two cases. In the first case he takes the image of the source in the horizontal plane. The resulting image is a source of the same strength and at the same distance below the ground plane. By putting a sink at $x = \infty$ he gets a half body and its image. This leads to a pressure distribution on the body as affected by the ground plane. The other case this author considers is the effect of an infinite vertical surface in the x direction. This gives rise to a source in one quadrant and its three images in the other three quadrants. This simulates the effect of a train passing a vertical wall or approximately another stationary train. He also gives calculations of the pressure coefficient C_p.

In the second theoretical method, a system of moving singularities is placed on the contour of the trains and within the body contour. This leads to a system of integral equations. These can be converted to a set of linear algebraic equations, which can be solved either by a Seidel method or by straight matrix inversion, depending on the size and complexity of the matrix.

Sockel (Ref. 4) has reported one such technique for two dimensional flow. He models the trains by a moving system of line vortices on the contour and a single source at the front end within the contours. This results in a semi-infinite boundary contour which is closed at the front end and open at the downstream end. By writing the equation of the stream functions for the singularities, he arrives at a set of integral equations. To complete the potential flow solution, it is necessary to have a condition on the net circulation about each train. A similar argument in wing theory leads to the Kutta condition. For his study, Sockel assumes that the net circulation about each train is zero. This assumption is expected to be increasingly valid for longer train configurations. The solution of the derived integral equations gives the instantaneous flow field. Solution is effected by direct quadrature using a form of the trapezoidal rule.

1(b) Review of Experimental Data Available in the Current Literature

There are not many reports of experimental data of the pressure field due to passing of high speed trains in the open literature. Fukuchi (Ref. 3) has reported field measurements of velocity and pressure due to the passage of a high speed train. The velocity was measured with a hot wire anemometer and the pressure with a pressure transducer. This would correspond to the "coach pulse". His measurements seem to indicate that the peak pressure pulse is not strongly affected by the height above the ground.

The main source of experimental data which has been uncovered to date, relating to this problem, is a paper by Hillmann et al (Ref. 5). They were involved in modifying an existing locomotive for high speed travel on the German railroad. Consequently they conducted extensive aerodynamic experiments to determine the effects of various shapes on the body pressure distribution. Experiments with models as well as full scale tests have been reported. Some of their results have been used for comparison in this report. They have also given an empirical method to account for the effect of crosswinds on the pressure pulse magnitude. One needs wind tunnel data for the specific body shape to be able to use the method.

2. DESCRIPTION OF THE PRESENT METHOD

The method adopted for the present computation is based on the work by A.M.O. Smith and J. Pierce (Ref. 6). It is an exact method capable of solving for the flow field about an arbitrarily shaped body in incompressible, potential flow. The method is quite general and can handle any number of bodies, thus accounting for mutual interference between bodies. Smith has given full details of the method as applied to single bodies. In the present work this has been extended to handle two bodies. Further, using the unsteady form of Bernoulli's equation, the pressure distribution around one of the bodies has been evaluated. This pressure distribution has been suitably integrated to arrive at forces and moments.

2(a) Basic Formulation

The method consists of placing a surface source-sink distribution on the contour of the bodies. The potential due to this distribution is written down. This contains both the self influence terms as well as the mutual influence terms. This results in a set of equations for the unknown source-sink distribution. This set of equations is solved using appropriate boundary conditions to give the source strengths. Once the source strengths are known, the potential at any point (either on the body or in free space) can be evaluated; from this the velocities and pressures can be obtained.

Although the basic method adopted is general and therefore can be readily extended, in principle, to three-dimensional flow cases, the overall aims of the present project precluded such a general formulation. In three-dimensional flow cases, significantly larger computing costs and additional computational difficulties, are to be expected. Consequently, the problem has been formulated and solved in two dimensions (see page 4).

The potential at any point p due to the source distribution around a shell of area S, bounded by $z = -\infty$ to $+\infty$ and $s = s_o$ to ℓ is

$$\varphi_p = \int_S \frac{\sigma dS}{r} \qquad (1)$$

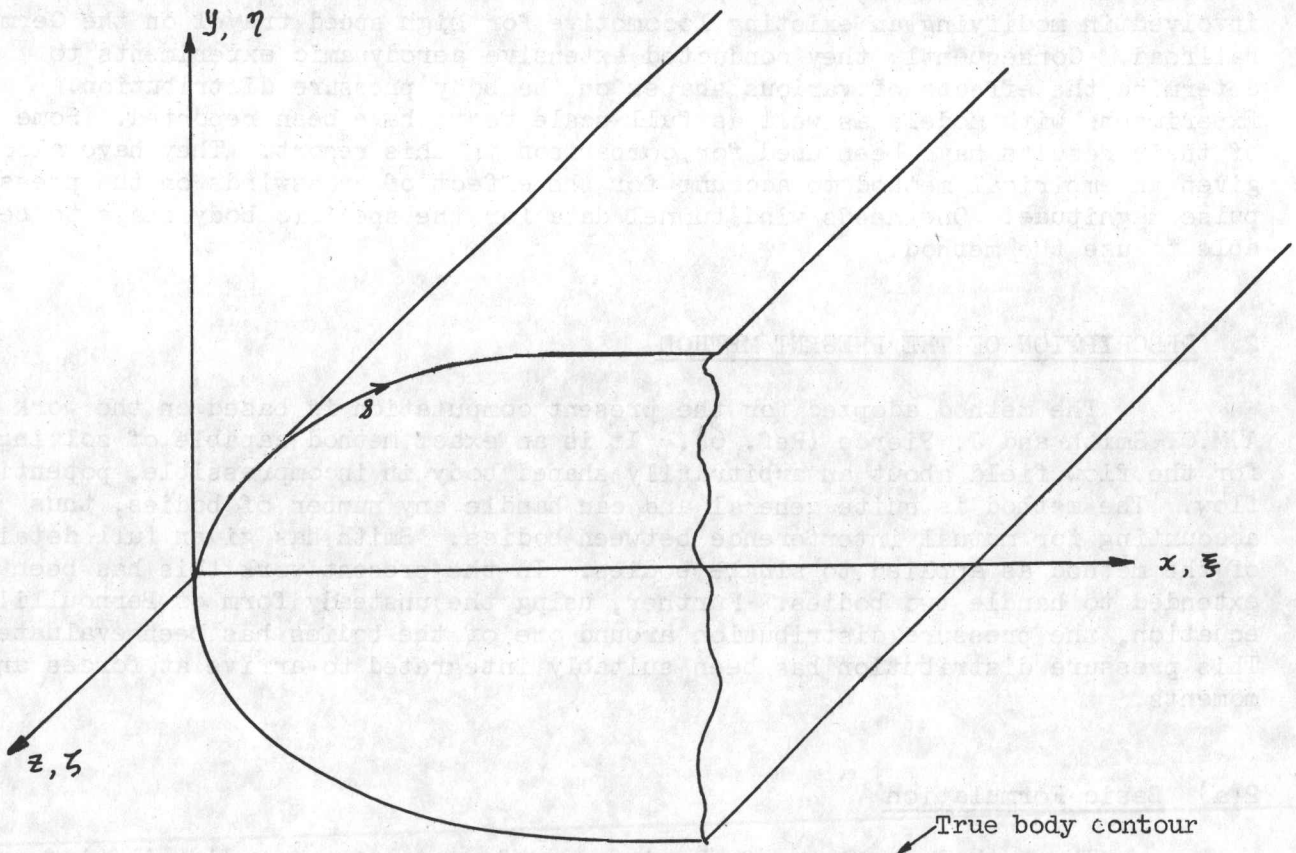
y, η
s
x, ξ
z, ζ

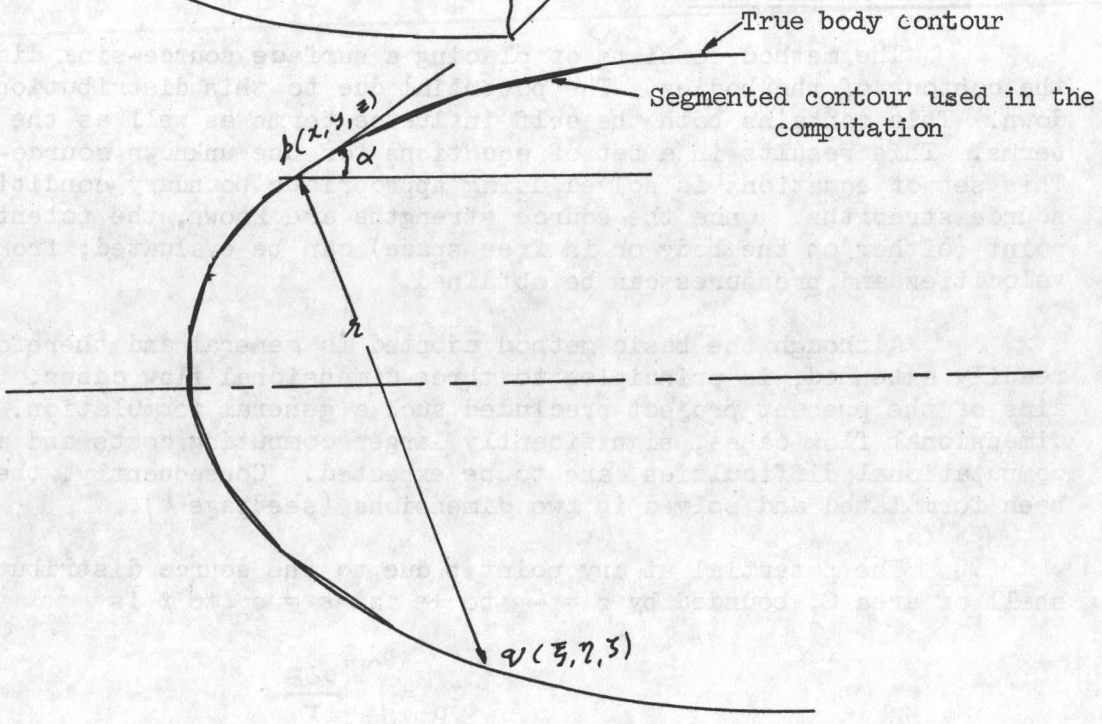
True body contour
Segmented contour used in the computation
p(x, y, z)
α
r
q(ξ, η, ζ)

If $p(x,y,z)$ (any field point) is in the plane $z = o$, and $q(\xi,\eta,\zeta)$ is any source point

$$r^2 = (x-\xi)^2 + (y-\eta)^2 + \zeta^2$$

and

$$\varphi_p = 2\int_{s_o}^{\ell}\int_{o}^{\infty} \frac{\sigma(s)\, d\zeta\, dx}{[(x-\xi)^2 + (y-\eta)^2 + \zeta^{1/2}} \qquad (2)$$

It can be shown that this reduces to

$$\varphi_p = -\int_{s_o}^{\ell} \sigma(s) \log\{(x-\xi)^2 + (y-\eta)^2\}^{1/2} ds$$

if we assume that $\sigma(s)$ does not vary in the z (or ζ) direction. (See Appendix). The computations of velocity and pressure involve derivatives of φ which are

$$\frac{\partial\varphi}{\partial x} = -2\int_{s_o}^{\ell} \frac{\sigma(s)\,(x-\xi)\, ds}{(x-\xi)^2 + (y-\eta)^2} \qquad (3)$$

$$\frac{\partial\varphi}{\partial y} = -2\int_{s_o}^{\ell} \frac{\sigma(s)\,(y-\eta)\, ds}{(x-\xi)^2 + (y-\eta)^2} \qquad (4)$$

Although up to this point the formulation has been made for one body, it is apparent that the presence of a second body merely increases the number of source points, if we decide to compute all the pressures and forces on only one of the bodies. It will give rise to a jump in the coordinates as one proceeds from one body to the other. This can be easily handled in a computer programme.

2(b) Transformation to Body Coordinates

Before proceeding to solve for $\sigma(s)$, it is necessary to get a relationship between s and the Cartesian coordinates (x,y). It is also preferable to perform the integrations in terms of s rather than x or y. The boundary s is broken up into a number of linear segments and some assumption regarding the variation of σ on each segment is made. In the present instance, two types of variation were tried. First, σ was assumed to be constant on each segment, but varying from segment to segment. Next σ was assumed to vary linearly on each segment as well as varying from segment to segment.

The following coordinate transformation used:

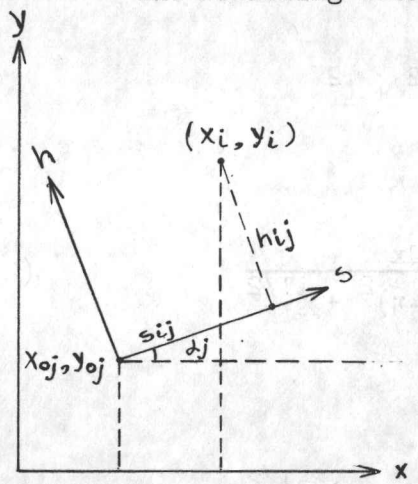

1. Body attached coordinates.
2. n is + outward normal to the body.
3. s is + clockwise around the body.
4. j the source point lies on the s axis.
5. i the field point arbitrarily located in space.

With the above transformation the integrals for the potential and its derivatives become (see Appendix):

$$\varphi(x,y) = -\sum_{j=1}^{n} \int_{s_j}^{s_{j+1}} \sigma_j(s) \log \{(s_{ij} - s)^2 + h_{ij}^2\}\, ds \qquad (5)$$

$$\frac{\partial \varphi}{\partial x} = -2 \sum_{j=1}^{n} \int_{s_j}^{s_{j+1}} \sigma_j(s) \frac{(s_{ij}-s)\cos\alpha_j - h_{ij}\sin\alpha_j}{(s_{ij}-s)^2 + h_{ij}^2}\, ds \qquad (6)$$

$$\frac{\partial \varphi}{\partial y} = -2 \sum_{j=1}^{n} \int_{s_j}^{s_{j+1}} \sigma_j(s) \frac{(s_{ij}-s)\sin\alpha_j + h_{ij}\cos\alpha_j}{(s_{ij}-s)^2 + h_{ij}^2}\, ds \qquad (7)$$

2(c) Boundary Condition

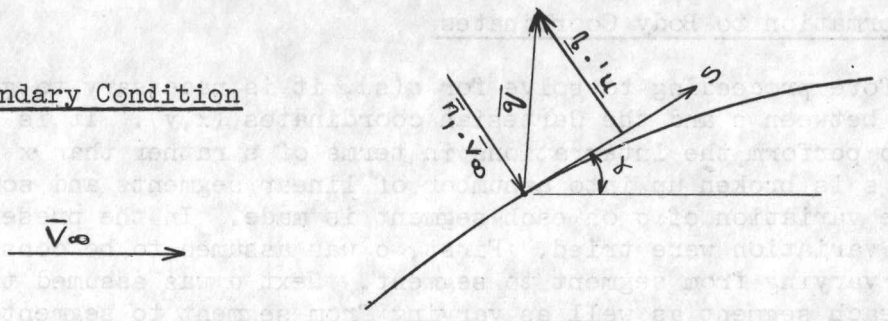

Consider the body moving to the left with a velocity $\bar{V}_\infty$ through a static fluid. The boundary condition (in potential flow) will be that the normal component of velocity will be zero on the boundary. This can be written as:

$$(\bar{q} - \bar{V}_\infty) \cdot \bar{n}_1 = 0 \qquad (8)$$

It should be noted that $\bar{V}_\infty$ has been introduced as a vector so that its direction can be specified. This is useful when computing crosswing cases.

2(d) Solution of the Equations

If we now make suitable assumptions regarding the variation of σ_j within each segment, equations (6) and (7) can be integrated. The first assumption that was tried was that σ_j is constant on each segment. The second assumption was that σ_j varied linearly on each segment.

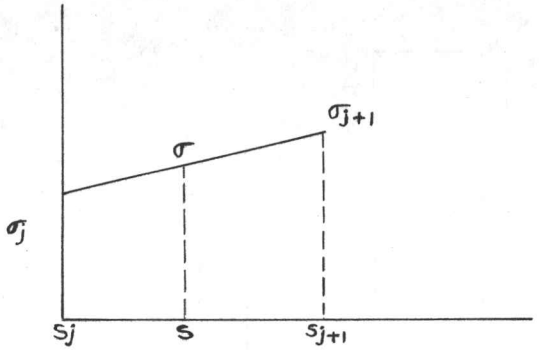

$$\sigma = a + b(s - s_{ij})$$

where a and b can be expressed in terms of s_j, s_{j+1}, σ_j, σ_{j+1}, and s_{ij}. After integrating equations (6) and (7), they can be arranged in the form

$$\frac{\partial \varphi_i}{\partial x} = \sum_{j=1}^{n} X_{ij}\sigma_j$$

$$\frac{\partial \varphi_i}{\partial y} = \sum_{j=1}^{n} Y_{ij}\sigma_j$$

From this the normal component of velocity on the body can be written as

$$\frac{\partial \varphi_i}{\partial n} = \sum_{j=1}^{n} \sigma_j \left[- X_{ij} \sin\alpha_i + Y_{ij} \cos\alpha_i \right]$$

This can be now used with equation (8) to solve for σ_j. One important point to be noted here is the case when i = j. For the case i = j, the integrals have to be evaluated by approaching the limits properly. If this is done $\partial\varphi/\partial n$ approaches the correct finite value. The procedure adopted in the present calculations was to solve for three basic cases. Subsequently these solutions can be superimposed to obtain solutions for any number of different cases including the effect of body crosswinds.

The basic cases considered are shown below. The bodies are assumed to be moving with unit velocity in the directions shown.

(1)

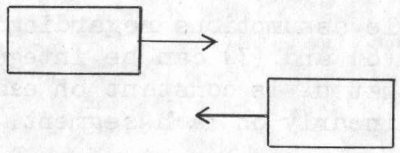

(2)

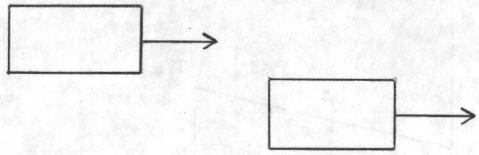

(3)

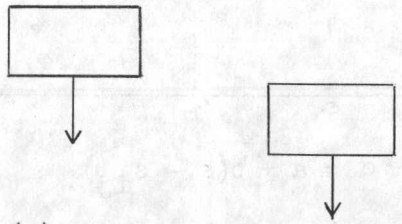

It is clear that case (1) by itself gives the solution when the two bodies are approaching each other. If cases (1) and (2) are superposed we get the solution for the case when one body is at rest and the other passes it. Superposition of all three cases gives the crosswind case.

2(e) Calculation of C_p

The pressure distribution can be obtained once the velocity distribution is known. The unsteady Bernoulli's equation is used.

$$\frac{p}{\rho} + \frac{1}{2} V^2 - \frac{\partial\varphi}{\partial t} = \frac{p_\infty}{\rho} + \frac{1}{2} V_\infty^2$$

$$\frac{p - p_\infty}{\frac{1}{2}\rho U^2} = C_p = \frac{V_\infty^2}{U^2} - \frac{1}{U^2}\left(V^2 + \frac{2\partial\varphi}{\partial t} \right)$$

Here U is a velocity used for nondimensionalizing the pressure. Normally, with only one body present, U can be chosen equal to V_∞. With two bodies, the choice is not obvious. In the present case it has been made equal to the closing velocity of the two bodies. $\partial\varphi/\partial t$ has been computed numerically

$$\frac{\partial \varphi}{\partial t} = \frac{\partial \varphi}{\partial x}\frac{dx}{dt} = U\frac{\partial \varphi}{\partial x}$$

By computing φ at least two stations $\pm \Delta x$ from the station x, $\partial\varphi/\partial x$ is obtained. In the present calculations $\Delta x = .01$ proved sufficient, i.e. no appreciable difference was found in φ by going from $\Delta x = .01$ to .001.

2(f) Computation of Forces and Moments

The drag force F_x, the side force F_y, the Yawing Moment YM and the Rolling Moment RM have been calculated by suitable integration of the pressure coefficient Cp.

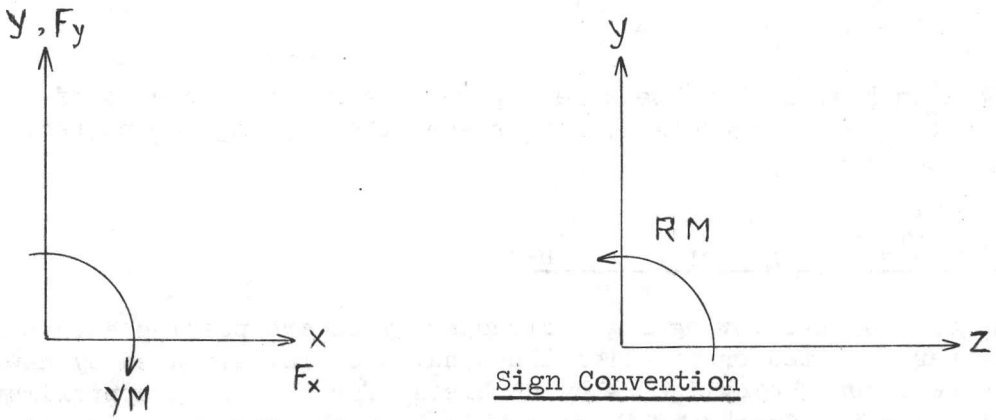

A simple trapezoidal rule has been used to integrate Cp. The pressure distribution has been assumed to be uniform in the z direction. The height of the train has been programmed as an input variable. The actual height used for computation is 85% of the height read in. This is to approximately account for the three-dimensional relief at the top of the train. For calculating the rolling moment, the centre of pressure in the z direction has been assumed to be at one third the height of the train from the ground.

3. RANGE OF COMPUTATIONS

A fairly extensive range of computations have been carried out. Apart from the cases of one and two cylinders, used for establishing the validity of the computations, four different body configurations (Fig. 4) have been utilized.

They all have a basic length of 360". The first three are 90" wide and the last is 120" wide. The basic configuration is rectangular with 15" corner radii. The first modification has elliptic front and rear sections joined by a rectangular section. The second and third modifications are rectangular with corner radii of 30" and 20" respectively. The height of the bodies was assumed to be 120" for all overall force and moment computations. The lateral separation between bodies was varied from 12" (between adjacent sides) to 48". A number of velocities from 45 mph to 150 mph were considered. Crosswinds of velocity 30 to 60 mph were considered at various angles from 0 to 90°. Cases with one body stationary and the other moving past it were also computed. The entire range of cases computed are shown in Tables 1 to 5.

4. RESULTS AND DISCUSSION

4(a) Motion of a Single Cylinder

The pressure distribution on an isolated single cylinder moving in an undisturbed fluid has been well established theoretically as well as experimentally. Hence this was used as an initial check on the accuracy of the developed numerical procedure. For a single cylinder in potential flow, moving with a velocity V_∞, the pressure coefficient is

$$C_p = \frac{p - p_\infty}{\frac{1}{2}\rho U_\infty^2} = 1 - 4 \sin^2\theta$$

This is plotted in Fig. 1. In the same figure is shown the results of the present computation using 36 points. It is seen that the agreement between the two solutions is excellent.

4(b) Two Cylinders Moving Past Each Other

The case of two moving right circular cylinders passing each other with their centers located on parallel lines has been investigated by Kawaguti (Ref. 2). He replaces the cylinders by doublets (for the first approximation). Then by considering the images of these doublets in the two cylinders he proceeds to higher order approximations. By summing the potential due to each of the doublets and their images, he arrives at a series solution. The accuracy of the solution depends on the number of terms of the series one considers. Kawaguti has given the solution to the fifth order approximation. This is shown plotted in Fig. 2 as a time history of the pressure at point A on one of the cylinders. On the same figure are also plotted the results of the present computation. To check the rate of convergence of the present solution a series of computations were undertaken, gradually increasing the number of points (or segments) considered. These results are also shown in Fig. 2. It is seen that the most critical point is at Ut/a=0. At this point, the present solution gave an asymptotic value of $C_p = -3.8$. This is seen in Fig. 3. Kawaguti's solution gave a value of -3.77. The 60 point solution is in error by less than 3% (based on the difference between the C_p at point A of the single body and the C_p at the same point with 2 cylinders at Ut/a=0). In the same figure is also shown the results of the computation when the source strength $\sigma(s)$ was assumed to vary linearly on each segment. It is seen that

the solution is not improved. Since this assumption also resulted in longer computing time, it was decided to use the assumption σ = constant on each segment for all succeeding computations.

The results for the two cylinder case are also indicative of the large interference effect present when the two cylinders are close together. The characteristic shape of the curve is also worth noting as it is roughly similar to the shape predicted for train passing cases.

4(c) Cab and Coach Pressure Pulses for Basic Geometry

Before discussing the cab and coach pressure pulses, it is useful to examine the pressure distribution on a body as it is approached and passed by an identical body moving with equal velocity. Figures 23(a) to (j) show the pressure distribution on a body with the basic configuration under such a condition. Figure 23(a) shows the isolated body moving with no interference from the approaching body. The pressures have been normalized using the closing velocity of the bodies. The pressure distribution shows the characteristic suction peaks at the corners as one would expect, which gradually approach atmospheric pressure near the middle of the body. As the interference due to body B is experienced on body A, the higher pressures ahead of body B tend to reduce the suction pressure at the front inside corner of body A. This type of pressure distribution is displayed until the front of body B is past the middle of body A. Subsequently, the suction pressures on the inside wall of body A increases further. When the two bodies completely overlap, a large suction pressure at the front and rear of the inside wall effectively seal the pressures on the inside wall maintaining a nearly uniformly high negative value. The pressure distribution will be symmetrical in time about the instant where the trains are completely overlapped. The pressures on the outside wall, i.e. not adjacent to the other train, are not greatly affected by the interference of the second train.

Figure 5 shows the time history of pressure at point 8 (located at the front of body A (see Fig. 4) on the side facing body B) on body A. The two bodies A and B are moving past each other with velocities V_A and V_B respectively, V_A being equal to $-V_B$. The closing velocity is therefore $2V_A$. The train pressure coefficient is based on the closing velocity. In the case of the moving cylinders, however, the pressure coefficient is based on the velocity of a single body to facilitate comparison with theoretical results. The point 8 on the body A corresponds to the location where $-C_p$ reaches a maximum value with only body A present and moving with velocity V_A. This can be defined as the cab pulse. The difference between the C_{pMAX} on this body and on the single cylinder is due to the different velocities used for non-dimensionalizing the pressures.

Some of the characteristic features of the pressure pulse at this point are as follows.

In the quiescent state, i.e., when mutual interference is absent, the C_p at this point will be -.75. As the trains approach each other, depending on the closing velocity, the mutual interference due to the two bodies will begin to relieve this suction pressure. As the head of train B passes the point 8 on train A, this relief is reduced until, by the time the

two trains are completely overlapping each other, the suction pressure again increases reaching a peak value of nearly -1.3 (for $\Delta y = 105"$). The actual curve followed is dependent on the lateral separation between the trains. This will be discussed in Section 4(j). The shape of the curve is roughly similar to the one shown in Fig. 2 for the moving cylinders. As predicted by theory, the curves will be symmetrical about $-Ut/\Delta y = 0$. The pressure-time history for point 19 (located at the middle of train A on the wide facing train B) as the two bodies approach and pass with equal velocities, is shown in Fig. 7 for the basic geometry. This corresponds to the coach pulse. The pressure in the quiescent state at this point depends on the length of the body. Theoretically, if the body were long enough, the effect of the frontal shape which gives rise to a large suction peak will have vanished and C_p would be zero. In the present case, a small suction pressure is still maintained. As the two bodies come closer together, the pressure time history at point 19 follows generally the same trends as for the cab pulse. Since the pressure at the quiescent state is not as high as at point 8, the consequences of the coach pulse are not as extreme as that due to the cab pulse.

4(d) Pressure Pulses When One Body is Stationary and the Other Moves Past It

The pressure time history at point 19 with the basic geometry when one of the bodies is stationary and the other moves past it with velocity V_B is shown in Fig. 9. There are two aspects to this case. Either body A could be moving and body B stationary or vice versa. In each case the pressure is given on body A. The pressure pulse at point 19 again corresponds to the coach pulse. This case is of interest because most experimental data on the pressure pulses gathered to date correspond to this case, specifically where the measurements are made on a wall as a train passes by. This will be examined in detail further on.

Referring to Fig. 9 it is seen that the case where $V_A = 0$ and train B moves past train A is a critical one. The pressure at point 19 undergoes a change in sign. As the train B approaches the train A, the pressure at point 19, which in the quiescent stage is atmospheric, starts to increase positively, i.e., the pressure will tend to push the side inwards. Just as the head of the train B moves past point 19, the pressure suddenly changes sign and as the trains completely overlap, reaches a negative maximum which would tend to pull the sides out. It is this reversal in sign of the pressure loading which probably could be more critical than a larger pressure pulse acting continuously in only one direction.

4(e) Forces Due to Train Passage

As mentioned in Section 2(f) the pressure distribution on body A has been suitably integrated to arrive at overall forces and moments. For an isolated body due to the nature of the present analysis (potential, non-circulatory flow) the integrated pressure distribution will be zero. However, in the presence of another body, there will be a net unsteady effect which does not integrate to zero. This is clearly seen in Fig. 12 where the force time history on body A is shown when bodies A and B move past each other with equal and opposite velocities. The nature of the curve is somewhat similar to the coach pulse time history (Fig. 7). The bodies will be subjected to a

fairly large amplitude (of the order of several tons) sideforce tending to push them together. The pulse duration is of the order of 100 millisecs giving a frequency of about 10 cps.

In Fig. 13 is shown a similar plot for the case of one stationary train and the other moving past it. The force on the stationary train as well as on the moving train are shown. Just as in the case of the pressure (at point 19 discussed earlier, see Fig. 9) the force on the stationary train is more critical. Not only does the force change sign, but the peak magnitude is also greater. Axial forces (in the x direction) are considerably smaller and have not been shown.

4(f) Effect of Lateral Spacing

Forces and pressures are generally relieved as the lateral distance between the bodies (Δy) is increased. In Fig. 5 the effect of lateral spacing on the pressure time history at point 8 on the basic geometry is shown. The basic shape of the curves are the same. The point to be noted is that the overall variation of pressure about the quiescent state is reduced. It is slightly different for the coach pulse. Here the effect is simply to reduce the $-C_{pMAX}$. This is shown in Fig. 7. Figures 10 and 11 show the variation of the peak suction pressure at a particular point as a function of lateral spacing. The relief afforded by larger spacing is greater for the coach pulse than for the cab pulse.

In Fig. 14, the integrated force F_y has been plotted as a function of lateral spacing. This graph clearly indicates the accelerating growth of the side force as the lateral distance separating the trains is decreased. For the basic geometry, with $V_A = -V_B = 90$ mph, increasing the lateral spacing from 15" to 24" reduces the side force by 4000 lb., whereas increasing the spacing from 12" to 15" reduces the side force by 3000 lb.

4(g) Effect of Streamlining

The effect of streamlining is also to relieve the loads and moments. This is shown by the computations carried out using the Modification 1 (Ellipse) geometry. This shape is made of an elliptic front and rear section and a rectangular midsection. For this geometry, when the body is moving without interference, the peak $-C_p$ occurs at point 10 (Fig. 22). The peak C_p value is -0.23 as compared to -0.75 on the basic geometry. The time history of the cab pulse, generated as two bodies with this streamlining approach each other and pass, is shown in Fig. 6. It is seen that the pressure variation is not as large as for the basic geometry. The coach pulse time history for this geometry is shown in Fig. 8. As would be expected the streamlining does not affect the coach pulse as much as the cab pulse, the former being influenced by the length of the train.

Figures 10 and 11 show the effect of lateral separation on both the cab pressure pulse and coach pressure pulse for a streamlined body. The cab pulse is seen to be much smaller for the Mod. 1 geometry and the rate of decrease of the cab pulse with an increase in Δy is slightly higher than for the basic geometry. A similar graph for Mod. 2 is seen to lie in between the

basic geometry and Mod. 1 as would be expected. As mentioned earlier the coach pulse is not strongly affected by frontal shape. This is also evident from Fig. 11.

The integrated pressure or force F_y for Mod. 1 and Mod. 2 geometries is shown in Fig. 14. The variation of total side force with spacing (Δy) is similar to that of the pressure pulses as discussed above.

4(h) Effect of Crosswind

Crosswinds have a very significant effect on the forces and moments acting during train passage. They tend to distort the pressure distribution to such an extent (depending on crosswind magnitude and direction) that force time histories have a totally different shape. This is shown in Fig. 17 where the time history of F_y has been plotted with crosswind angle as a parameter. In addition the case of no crosswind is also shown in the same figure for comparison.

When there is no crosswind, the isolated body does not experience a net force. As the bodies move closer together, the mutual interference distorts the pressure distribution asymmetrically and a net force results. The significant lateral force (directed towards the passing train) is negligible until the bodies are very close together. With a crosswind (see Fig. 17) starting at a crosswind angle of 0°, i.e., wind blowing from left to right, it is seen that the train is subjected to a force which varies in direction as the trains approach each other and pass. The net force tends to rise positively as they approach each other, reaching a peak when the nose-to-nose distance between the bodies is nearly zero. As they start overlapping each other the force starts decreasing and ultimately becomes negative. The negative maximum is reached when the bodies are halfway across each other. Thus, even though the crosswind may not significantly increase the peak value of force, the fact that the train is subject to a significant lateral force whose sign changes rapidly is of importance. The effect of varying the crosswind angle is to change the amplitudes of the force peaks. The maximum amplitudes seem to be reached with a crosswind angle between 60° and 75°. The distortion of the pressure distribution due to crosswinds also results in a net force in the x direction, i.e., either a net thrust or drag depending on the crosswind angle. This is shown in Fig. 18. The magnitudes are not large enough to have much significance.

Crosswinds seem to affect the net yawing moment very strongly. The yawing moment time history is shown plotted in Fig. 19 when two trains approach each other and pass (with equal and opposite velocities of 60 mph) in the presence of a crosswind of 45 mph magnitude blowing at an angle of 75°. Again for comparison, the case when no crosswind is present is shown in the same figure. The crosswind gives rise to a peak yawing moment greater than 10 times that with no crosswind. The same case for the streamlined body shape (Mod. 1) is also shown in Fig. 19. It is seen that the streamlining relieves the yawing moment considerably.

A final point to be noted regarding the effect of crosswinds is that it depends on the longitudinal separation distance Δx. This is brought out in Fig. 20. It is seen that when Δx is zero, the crosswind angle has negligible effect. When $\Delta x \simeq 341$ inches, i.e., when the trains are first commencing to overlap, the crosswind has a significant effect.

4(i) Problems of Scaling

Scaling for experimental purposes appears to be a difficult problem. This is due to the essential nonlinearity of the interference between the trains. This is the fundamental difference between the pressure distribution on a single isolated body moving with uniform velocity and that on bodies subjected to mutual interference. This can be seen in the form of the Bernoulli's equation. The general Bernoulli's equation for unsteady flow is:

$$p + \frac{1}{2}\rho V^2 - \rho \frac{d\varphi}{dt} = p_\infty + \frac{1}{2}\rho V_\infty^2$$

$$\frac{p-p_\infty}{\frac{1}{2}\rho V_\infty^2} = 1 - \frac{V^2}{V_\infty^2} + \frac{2}{V_\infty^2}\frac{d\varphi}{dt}$$

In the case of steady flow $d\varphi/dt = 0$ and hence pressure (or force) can be scaled in proportion to the square of the free stream velocity. In the case of unsteady flows the $d\varphi/dt$ term which is dependent on the interference is not proportional to (velocity)^2 in general. In fact under certain conditions it is nearly proportional to the velocity. This is shown in Figs. 15 and 16. F_y is shown plotted against velocity for the basic geometry when the trains completely overlap each other. It is seen that F_y is almost directly proportional to V. In fact, it appears from Fig. 16 (which has been drawn to a highly exaggerated scale) that $F_y \alpha (V)^{.915}$. This is only at $\Delta x = 0"$. When the bodies are far enough apart $F_y \alpha (V)^2$. In between these two extremes it is difficult to predict exactly what the scaling factor will be. This is shown in Fig. 12 where the force time history for the basic geometry has been plotted for different velocities. When one includes any crosswind effects, the problem becomes more difficult.

4(j) Comparison of Present Results with Those of Sockel

As mentioned in the literature review, Sockel (Ref. 4) has reported a theoretical investigation of the pressure distribution along passing railroad trains. Some of his results will be used for comparison with the present computations.

Sockel's results have been presented for two-dimensional bodies, semi-infinite in length with a circular nose section. The lateral separation distance is 1.3 times the width of the trains. Some of the graphs from his paper are shown in Figs. 21(a) to (d). Figure 21(a) shows the pressure distribution on body A as bodies A and B approach each other with equal velocities and overlap. Since his bodies are semi-infinite they can never completely overlap. Figures 23(a) to (j) show the corresponding pressure distribution obtained from the present computations. The present computations shown are for the basic geometry with a lateral separation of 105" or 1.167 times the train width. Consequently the comparison can only be qualitative. It should also be noted that Sockel has normalized his pressure distribution with the velocity of one of the bodies while the present computations have used the closing velocity.

For the isolated body (Figs. 21(a) and 23(a)) the pressure distributions are similar, with a lobe of positive pressure (inward arrows in present case) in the front and two lobes of negative pressures on the front corners. In the present case, of course, the pressure distribution will be symmetrical about both axes. The pressure distribution when the two bodies are just opposite each other is shown in the second figure from the top in Fig. 21(a). The corresponding case in the present study is shown in Fig. 23(b). Both these figures indicate a region of +ve pressure at the front followed by a small region of -ve pressure and subsequently +ve pressure. The third contour (from the top) in Fig. 21(a) corresponds to Fig. 23(e) in the present computations. Some of the common features are a region of +ve pressure at the front, followed by a -ve pressure over a fairly long length and then a final +ve pressure region. Beyond this point it is not possible to compare the two solutions because of the type of bodies. The present computations show that the -ve pressure extends on the inner side until it reaches a peak value at $\Delta x = 0$ when the trains overlap completely. At this point the large negative pressures at either inner corner effectively block any relief and the pressure is almost uniformly negative all along the inner side.

Figure 22 shows the pressure distribution on the Mod. 1 configuration. As would be expected the peak pressure is less than for the basic geometry case and the pressure distribution is more uniform.

The main differences between Sockel's computation and the present are seen from a comparison of the pressure signatures at a particular point. His curves for point 3 correspond roughly to the cab pulse of the present computation. In Fig. 21(b) the pressure signature for point 3 is given when two trains approach each other with equal velocities. This corresponds roughly to the pressure time history for point 8 in Fig. 5 at a $\Delta y = 114"$. It is seen that the curves are somewhat similar up to a $-Ut/\Delta y \simeq 1$. Beyond that, the present theory predicts a continued rise in -ve pressure ending in a peak at $Ut/\Delta y = 0$ whereas Sockel's curve tends to flatten out in that region. Similarly, in Fig. 21(d) Sockel shows the pressure pulse on the stationary train as the other train passes by. This is similar to the graph shown in Fig. 9. Again the comparison is valid up to $Ut/\Delta y \simeq 1$. The main reason for the differences noted above appears to be the difference in body shapes, Sockel using semi-infinite bodies and the present work being carried out with finite bodies.

4(k) Comparison with Experimental Data

Experimental results available are very sparse. Further, it is established that the interference results can be very sensitive to the numerous parameters involved, i.e., body geometry, spacing, velocity, type of measurement, and so forth. Wind tunnel results under steady conditions appear to be of limited use for predicting interference loadings since the real problem of interest (passing with relatively small lateral separations) is inherently unsteady in nature. Another important difficulty is the problem of scaling which has been discussed earlier. Keeping these points in mind, one can still examine the limited experimental data from a qualitative viewpoint.

The main source of experimental data appears to be that due to Hillmann et al (Ref. 5). Extensive (wind tunnel) model testing as well as

some very limited full scale testing has been carried out by these authors. Some general comparisons can be made using their results. The pressure signature of a train (moving at 125 mph) as it passed a stationary measuring train has been recorded and is shown in Fig. 24. This would correspond to the measurement of the coach pressure pulse. This is comparable to the pressure time history obtained from the present computations shown in Fig. 9 (for the case $V_A = 0$, $V_B = 125$ mph). It is not possible to compare the magnitude of the pressure pulse as Hillmann et al do not give a scale for their pressure measurement. However, the shapes of the pulse are quite similar and the duration is of the same order of magnitude (about 200 msec).

In Fig. 25 is shown the effect of lateral spacing on the coach pressure pulse as given by Hillmann et al. The locomotives 112 and 103 referred to are roughly similar in shape to the present basic geometry and the Kruckenburg model used is similar in shape to the Mod. 1 geometry used for the present calculations. This figure can be compared to the results predicted by the present computations shown in Fig. 10. It is seen that the shape of the curves is similar in both cases and the effect of streamlining is of the same order of magnitude in both cases.

The problem of scaling discussed in Section 4(i) can be also substantiated from Fig. 26. In this figure are shown the results of Hillmann's tests to determine the relationship of the magnitude of the pressure pulse to the train velocity. It is apparent that the pressure pulse magnitude is definitely not proportional to $(\text{velocity})^2$.

Hillmann et al have reported a measurement of the pressure pulse under crosswind conditions. This is also shown in Fig. 24. It is seen that crosswind distorts the shape of the pressure pulse in a manner similar to that indicated by the present computation (Fig. 17).

4(ℓ) Limitations of the Present Study

There are two main limitations regarding the present study. One is due to the scope of the work and the other the type of approach used. These will be elaborated on below.

By scope of the work, one is referring to the fact that the solution is in two dimensions. Consequently, the pressure relief afforded by the third dimension is not included. This is vividly brought out in Kawaguti's work (Ref. 2) where he considers the pressures due to passing cylinders and those due to passing spheres. The peak suction pressure at a particular point on the cylinders reaches nearly -3.8. For a similar case when two spheres are passing, the peak pressure at the same point is only -1.55. Thus one can appreciate the relief of pressure afforded by the third dimension. In the case of elongated bodies such as the ones used in the present study, the relief will not be so great everywhere. Near the ground plane, there will be practically no relief. The pressures will begin to taper off as one approaches the top of the train. An empirical approach to include this effect has been used in the computation of the moments and forces.

The second major limitation is due to the type of solution used in the present study. It is based on potential flow. Consequently, all the viscous effects have been neglected. Viscous effects as is well known will

be confined to the boundary layer on the bodies and its major effect will be felt near the rear of the trains where the flow will separate from the bodies giving rise to a large amount of drag which cannot be accounted for by potential flow theory. The pressures at the rear corners will also not be as high as predicted by potential flow theory. All these factors will lead to the present solution predicting conservative loads. The loads in practice might lie in between two-dimensional and three-dimensional solutions. Finally, one should note the limitations of the solutions regarding the number of segments or points chosen for the computations. In the present instance it has been observed that the solution is fairly sensitive to the number of points and their distribution. To arrive at a solution which approaches the asymptotic solution, a minimum of 72 points were needed. Increasing the number of points will increase the accuracy of the solution, but it will also increase computing time which soon could become prohibitive depending on the number of cases one wants to compute. The present solution is within 5% of the asymptotic solution. One of the features of the present study is that only 3 basic cases have to be computed in detail for each configuration and separation distance. Once these are complete the superposition of the solution discussed in Section 2(d) reduces costs enormously.

5. CONCLUSIONS

General conclusions that have been reached during the present study are as follows:

1. An incompressible potential flow method in two dimensions has been developed, capable of predicting the unsteady pressure distribution, forces (side force and drag), and moments (yawing and rolling) on moving or stationary bodies (e.g., trains) of arbitrary shape, due to the passage of a second body. Effects of arbitrary wind velocity may also be included.

2. Substantial aerodynamic pressure pulses are imposed due to the passage of a train past another moving or stationary train. For example, for the basic geometry considered, with a lateral separation of 105" (train width 90") a pressure coefficient, based on closing velocity, at the front of the train (point 8) of nearly 1.4 and an integrated load of 9000 lbs is predicted due to the passage of another train with equal and opposite velocity of 60 mph.

3. The case of a stationary train encountering a pressure pulse due to the passage of another moving train appears to be the critical one. This is due to the sudden reversal of the direction of the pressure loading. For example, for the basic geometry, with a lateral separation of 105", the pressure coefficient on the stationary train at point 19 (i.e., middle of the train) changes from +.6 to -1.4 in about 75 milliseconds (for a train velocity of 125 mph). This impulsive loading can be quite abrupt. Initially it will act so as to push the sides and windows of the train inwards, then it abruptly reverses, loading the train sides in the opposite direction.

4. The lateral separation Δy, between passing trains is a very important factor affecting the interference loading. Increasing Δy reduces this

loading rather quickly when the separation is small and less rapidly at larger separation. The amount of reduction is dependent on body shapes, train velocities, and the nose-to-nose distance between the trains.

5. Body shape plays a very important role in deciding the type and magnitude of the interference loading. Streamlining can reduce the loading significantly. Typically, for identical cases of lateral separation and velocity, the maximum cab pressure pulse on Mod. 1 geometry (elliptical nose and rear sections) is reduced to a value of $C_p = -0.90$ from a value of $C_p = -1.40$ for the basic train geometry. The integrated interference loads are also similarly reduced.

6. Crosswinds can significantly increase the magnitude and type of loading due to train passage. For example, in the case of two trains approaching each other and passing with equal velocity, the sideforce is predominantly in the positive direction, i.e., tending to pull the trains together. If there is crosswind the trains are initially subject to a significant positive load which gradually changes sign and becomes significantly negative and then as the trains overlap, becomes strongly positive again.

7. For the case of two trains approaching and passing each other with equal velocity, the crosswind effect was found to be greatest, for a given crosswind strength, when the crosswind angle was approximately 70° (relative to direction of train travel).

8. Crosswinds can significantly increase the interference yawing moment. Streamlining will tend to alleviate crosswind effects significantly.

9. Scaling of the interference loads, measured or predicted, applicable to closely passing trains, from one set of velocity conditions to another set, presents inherently important difficulties. This follows directly from the basic unsteady nature of the problem and the fact that there is no simple (moving) coordinate system in which the problem may be considered as stationary. Thus the singularities representing the flow boundaries have variable strength (w.r.t. time) in all useful coordinate systems and the $\rho\, \partial\varphi/\partial t$ term will always play an important role in establishing fluid pressures. The only expected exception to this will occur when the body separations are large and the problem then will be nearly steady in coordinate systems translating with the bodies. These situations, however, are not expected to be the critical design cases, so that in general it appears that ad hoc scaling "rules" will have to be developed based on measurements or calculations which bracket the complete ranges of interest, including the important role of crosswinds.

10. Wind tunnel studies under steady state conditions in general will be quite inadequate for the prediction of the true unsteady train interference loadings. Even for the case of a train passing a long plane wall, wind tunnel simulations with steady flow conditions will be severely hampered by the presence of the tunnel wall boundary layer if viscous body effects are of interest.

6. RECOMMENDATIONS FOR FUTURE WORK

The present study has brought to light the importance of the aerodynamic phenomena due to interference when two bodies with a high relative velocity and close lateral separation approach each other and pass. From the point of view of supplying preliminary data, the present work is satisfactory. It is capable of predicting the trends of such effects as streamlining, lateral separation crosswinds, etc. However, for a finalized design, measurements initially with scaled vehicles are essential. It is also clear that for model tests to be of real significance, unsteady interference effects will have to be accurately simulated. In fact, the lack of such data appears to be the major deficiency in our present understanding of real interference loadings. Wind tunnel tests under steady conditions can provide complementary information, however, as pointed out earlier, such testing has definite limitations for the present interference problem.

Regarding extensions to the present theoretical work, it can be expanded to include the third dimension. This would have to be approached with some caution as it would entail larger developmental and computational costs. Complemented by model (and possibly limited full scale testing) covering an adequate parameter range, the present study itself could be empirically modified to give three dimensional and real fluid effects.

REFERENCES

1. Carpenter, L. H. — "On the Motion of Two Cylinders in an Ideal Fluid", J. Res. Nat. Bur. Std., Vol. 61, No. 2, Aug. 1958, pp. 83-87.

2. Kawaguti, M. — "The Flow of a Perfect Fluid Around Two Moving Bodies", J. Phys. Soc. Jap., Vol. 19, No. 8, Aug. 1964, pp. 1409-1415.

3. Fukuchi, G. — "Application of Axially Non-Symmetric Half Bodies", Proc. 14th Ja-an Nat. Cong. Appl. Mech., 1964.

4. Sockel, H. — "Pressure Distribution Along Passing Railroad Trains", Zamp, Vol. 21, 1970, pp. 619-628.

5. Hillmann, W. et al — "Aerodynamic Experiments for the Development of the Locomotive '103' of the German Federal Railroad for High Speed Travel". Glasers Annalen, Vol. 92, No. 9, Sept. 1968, pp. 268-276, and continued in Vol. 92, No. 11, Nov. 1968, pp. 352-360.

6. Smith, A.M.O. Pierce, J. — "Exact Solution of the Neumann Problem. Calculation of Non-Circulatory Plane and Axially Symmetric Flows About or Within Arbitrary Boundaries". Douglas Aircraft Co. Report No. ES 26988, April 25, 1958.

BIBLIOGRAPHY

Grunwald, K. J. "Aerodynamic Characteristics of Vehicle Bodies at Crosswind Conditions in Ground Proximity". NASA TN D-5935, Aug. 1970.

Yamamoto, A. "Pressure Rise due to the Friction of a Train at the Entrance of a Tunnel". Quart. Rep. RTRI, JNR, Vol. 10, Nov. 4, 1969, pp. 224-225.

Miki, T. et al "On the Aerodynamic Problems of the High Speed Train". Bulletin JSME, Vol. 2, No. 6, 1959, pp. 355-364.

Ohukushi, J.
Nishimura, B. "Pressure Rise in Passenger Car in Tunnel (on existing narrow gauge line)". QR RTRI JNR, Vol. 11, No. 1, 1970, pp. 42-46.

Hara, T. "Aerodynamic Force Acting on a High Speed Train at Tunnel Entrance". Bulletin JSME, Vol. 4, No. 15, 1961, pp. 547-553.

Hara, T. et al "Aerodynamic Drag of Trains". QR RTRI JNR, Vol. 8, No. 4, 1967.

Hara, T. "Aerodynamic Drag of Trains in Tunnels". QR RTRI JNR, Vol. 8, No. 4,1967.

Fukuchi, G.
Nishiyawa, S. "Estimation of Aerodynamic Drag of a Train in a Long Tunnel". Quart. Rep. RTRI, JNR, Vol. 8, No. 1, 1967.

Woolard, H. W. "Slender Body Aerodynamics for High Speed Ground Vehicles". J. Aircraft, Vol. 8, No. 8, Aug. 1971, pp. 597-603.

Hara, T. et al "Aerodynamics of High Speed Train", IRCA-UIC "High Speeds" Symposium, Vienna, 1968.

Gaillard, M. "Measurements on Models for Determining the Air Drag and Pressure Distribution on Railway Trains in Tunnels", ZAMM, Vol. 16, No. 6, 1965, pp. 844-845 (German).

Colin, P. E. "Impulsive Pressures in the Train Passing Problem", Symp. on Road Vehicle Aerodynamics, City Univ. of London, No. 6-7, 1969.

Main, M. "Test and Measuring Apparatus for Determining by Experiment the Pressure Wave Caused by Different Locomotives Passing Stationary Groups of Rolling Stock", Glasers Annalen, Vol. 93, No. 12, Dec. 1969, pp. 371-375 (German).

Gaillard, M. A. "Aerodynamical Deliberations and Discussions on the Experimental Investigation of the Pressure Wave Caused by Various Locomotives Passing Groups of Stationary Rolling Stock", Glasers Annalen, Vol. 93, No. 12, Dec. 1969, pp. 376-382 (German).

BASIC GEOMETRY

TABLE 1

Δy	105	105	105	105	105	105	105	105	105	105	105	105	105	105	105
Δx	0.0	20	340	360	380	52.5	78.75	105	210	420	262.5	315	341.25	472.5	630
V_A	45	60	90	135	150	45	60	90	135	150	0	0	0	0	0
V_B	45	60	90	135	150	0	0	0	0	0	45	60	90	135	150
V_C	0	0	0	0	0	0	0	0	0	0	0	0	0	0	0
$\theta°$	0	0	0	0	0	0	0	0	0	0	0	0	0	0	0
V_A	60	60	60	60	60	60	60	60	60	60	60	60	60	60	60
V_B	60	60	60	60	60	60	60	60	60	60	60	60	60	60	60
V_C	30	30	30	30	30	45	45	45	45	45	60	60	60	60	60
$\theta°$	30	45	60	75	90	30	45	60	75	90	30	45	60	75	90

N SEP = 15, NVE L = 3, H = 120 TOTAL CASES = 450

TABLE 2

Δy	102	102	102	102	102	102	114	114	114	114	114	114	138	138	138	138	138
Δx	0	25.5	51	102	204	306	0	28.5	57	114	228	342	0	34.5	69	276	414
V_A	45	60	90	45	60	90	0	0	0	60	60	60	60	60			
V_B	45	60	90	0	0	0	45	60	90	60	60	60	60	60			
V_C	0	0	0	0	0	0	0	0	0	45	45	45	45	45			
$\theta°$	0	0	0	0	0	0	0	0	0	30	45	60	75	40			

N SEP = 18, N VEL = 14, H = 120 TOTAL CASES = 252

Note: V_A, V_B, V_C are in mph; x, y, H are in inches.

TABLE 3

MOD. 1 (ELLIPSE)

Δy	105	105	105	105	105	105	105	105	102	114	138	102	114	138
Δx	0	26.25	52.5	105	210	315	525	735	0	0	0	204	228	276

VELOCITIES SAME AS FOR CASE 2
N SEP = 14, N VEL - 14, H = 120 , NUMBER OF CASES 196

TABLE 4

MOD. 2 (30" RADIUS)

Δy	105	102	105	114	138	102	105	114	138
Δx	1 body	0	0	0	0	204	210	228	276

VELOCITIES SAME AS FOR CASE 2
N SEP = 9, N VEL = 14, H = 120 , NUMBER OF CASES 126

TABLE 5

MOD. 3 (120" WIDE)

Δy	105	136
Δx	1 body	0.0

VELOCITIES SAME AS FOR CASE 2
N SEP = 2, N VEL = 14, H = 120 , NUMBER OF CASES 28

TOTAL NUMBER OF CASES: 450 + 252 + 196 + 126 + 28 = 1,052

NOTE: V_A , V_B , V_C are in MPH. x, y, H are in inches.

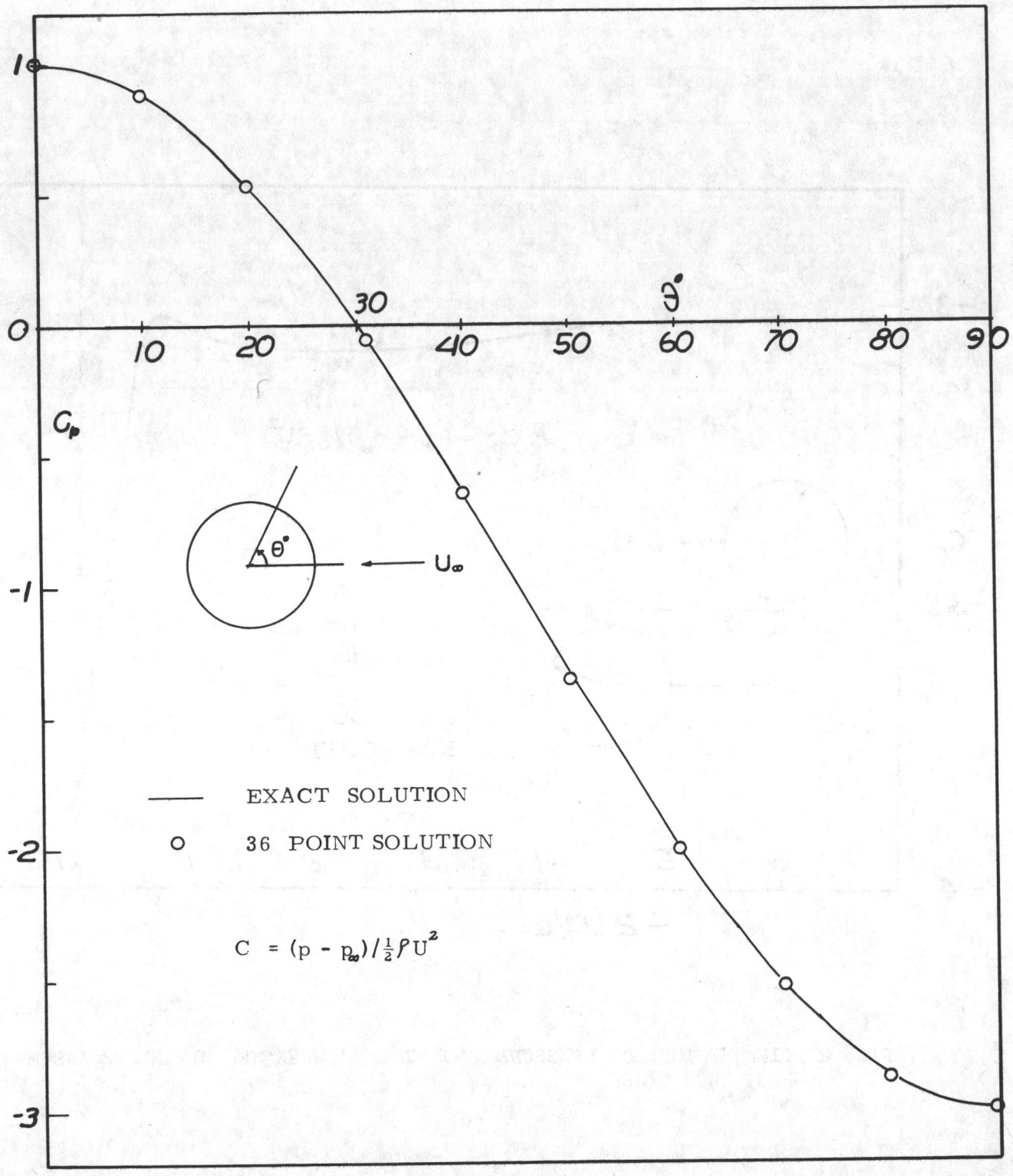

FIG. 1 PRESSURE DISTRIBUTION OVER A SINGLE CYLINDER

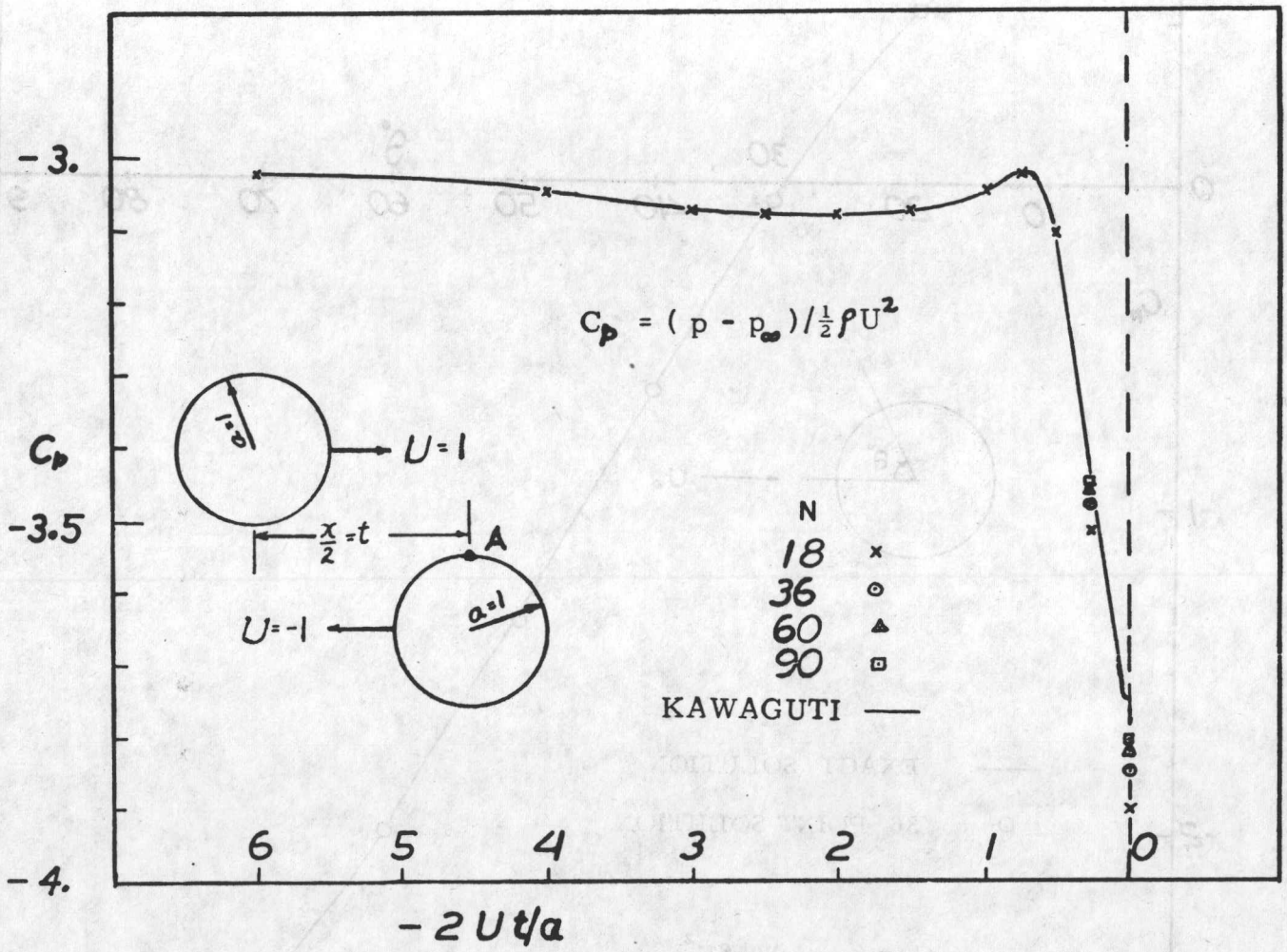

FIG. 2 TIME HISTORY OF PRESSURE AT POINT 'A' WHEN TWO CYLINDERS ARE MOVING PAST EACH OTHER

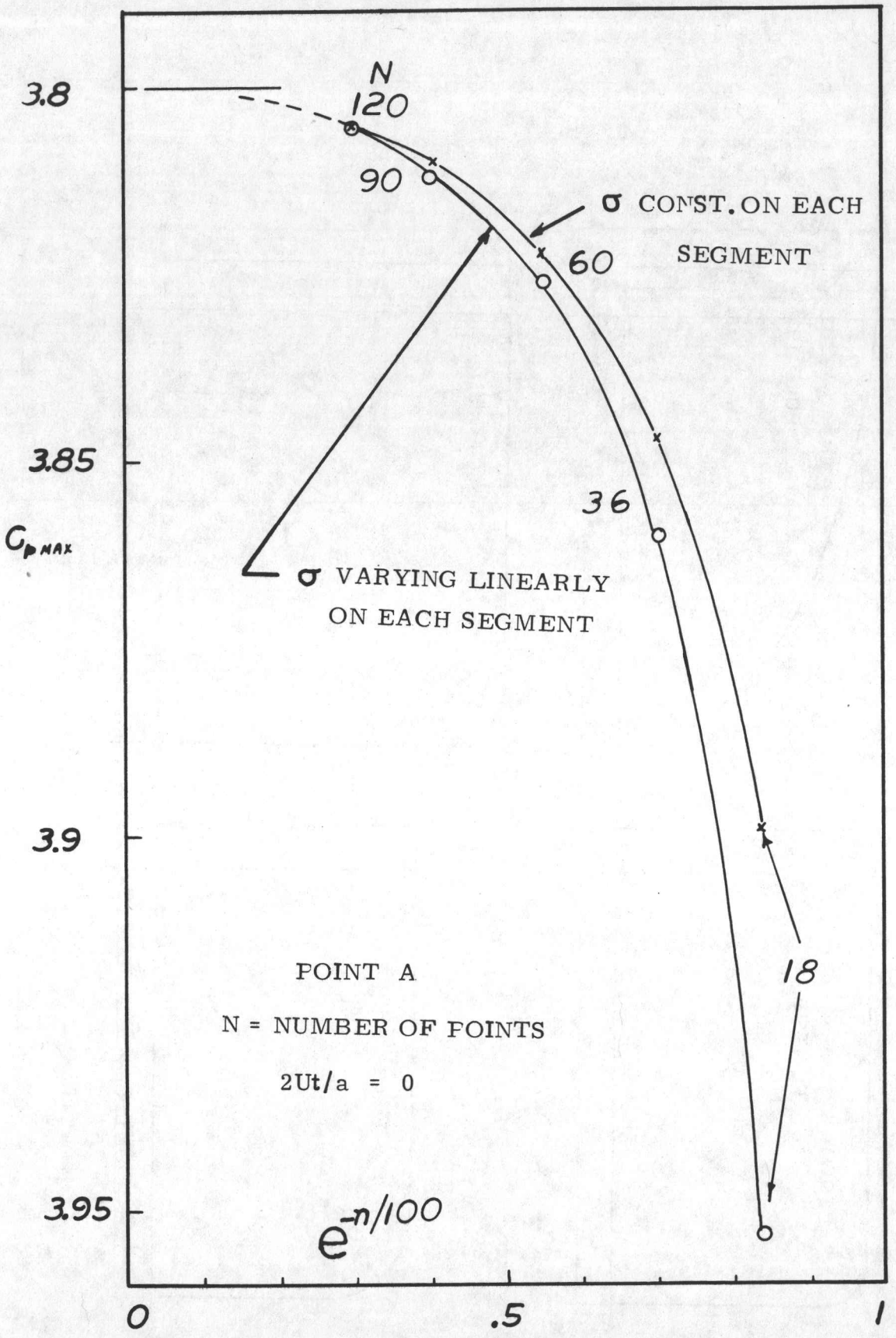

FIG. 3 RATE AT WHICH $-C_{pMAX}$ REACHES THE ASYMPTOTIC VALUE

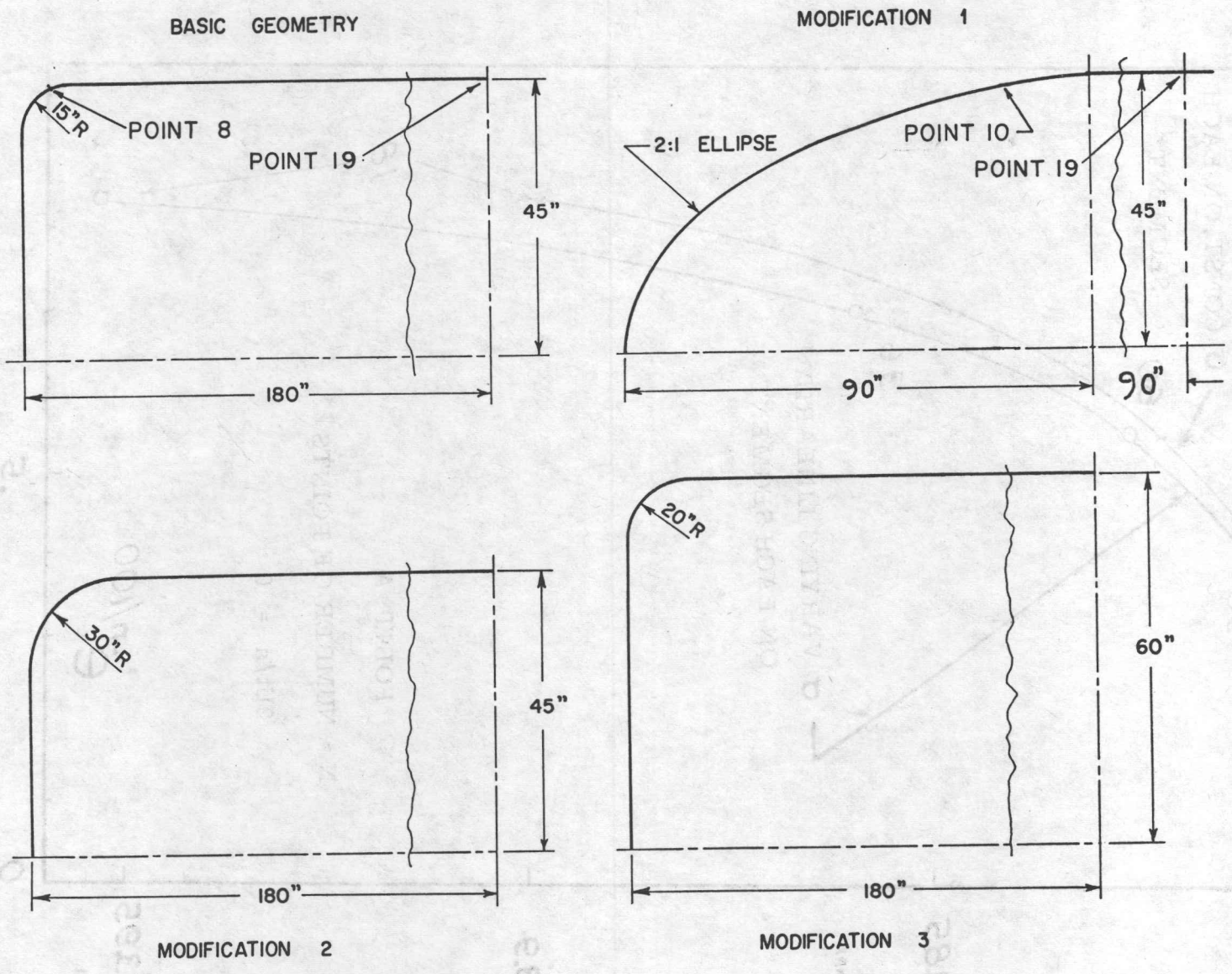

FIG. 4 DIFFERENT BODY SHAPES USED IN NUMERICAL STUDY (BODIES ARE SYMMETRIC IN ALL 4 QUADRANTS)

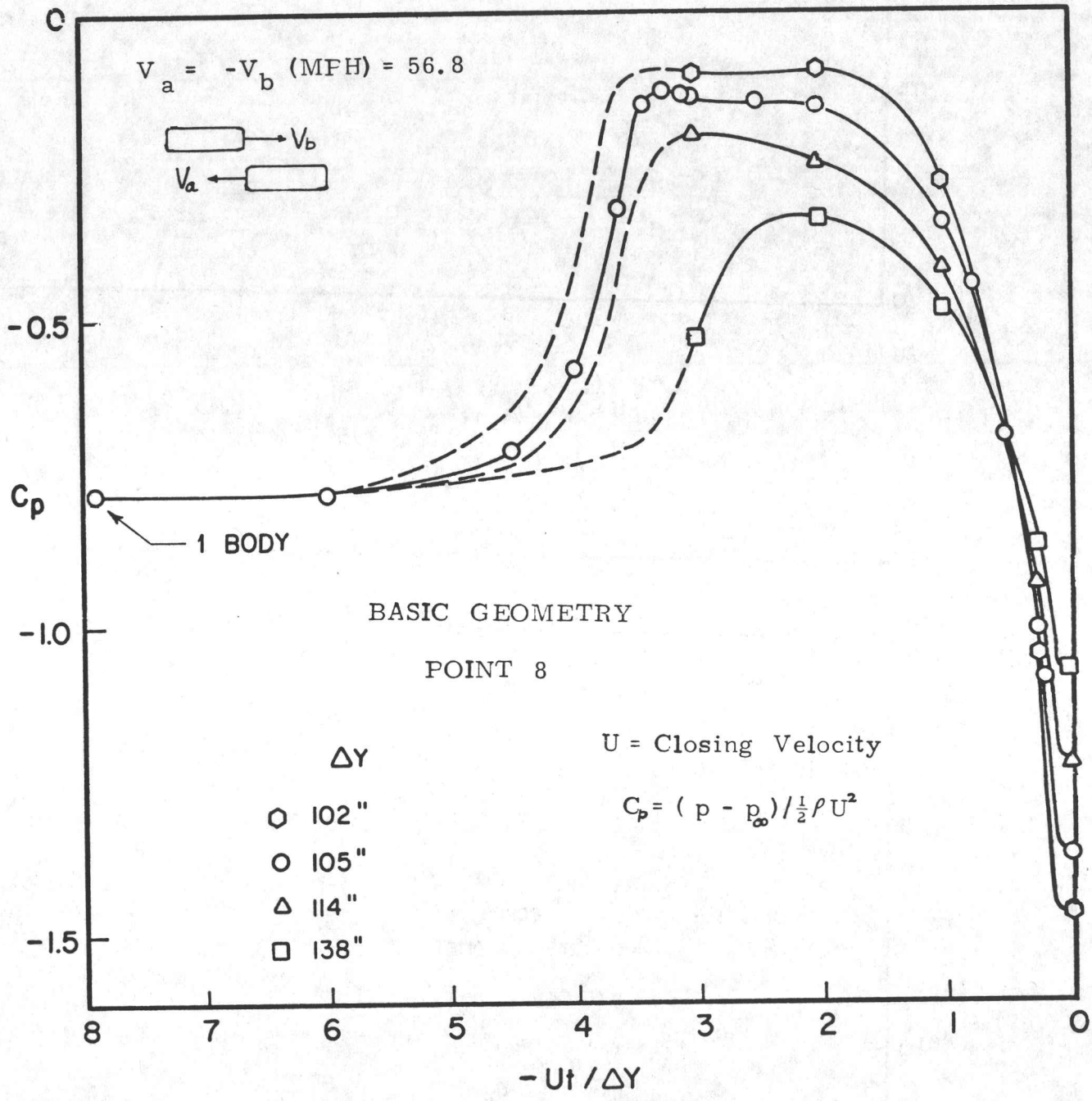

FIG. 5 TIME HISTORY OF PRESSURE AT POINT 8 (BODY A) WHEN TWO IDENTICAL BODIES ARE MOVING PAST EACH OTHER WITH EQUAL AND OPPOSITE VELOCITIES (BASIC GEOMETRY)

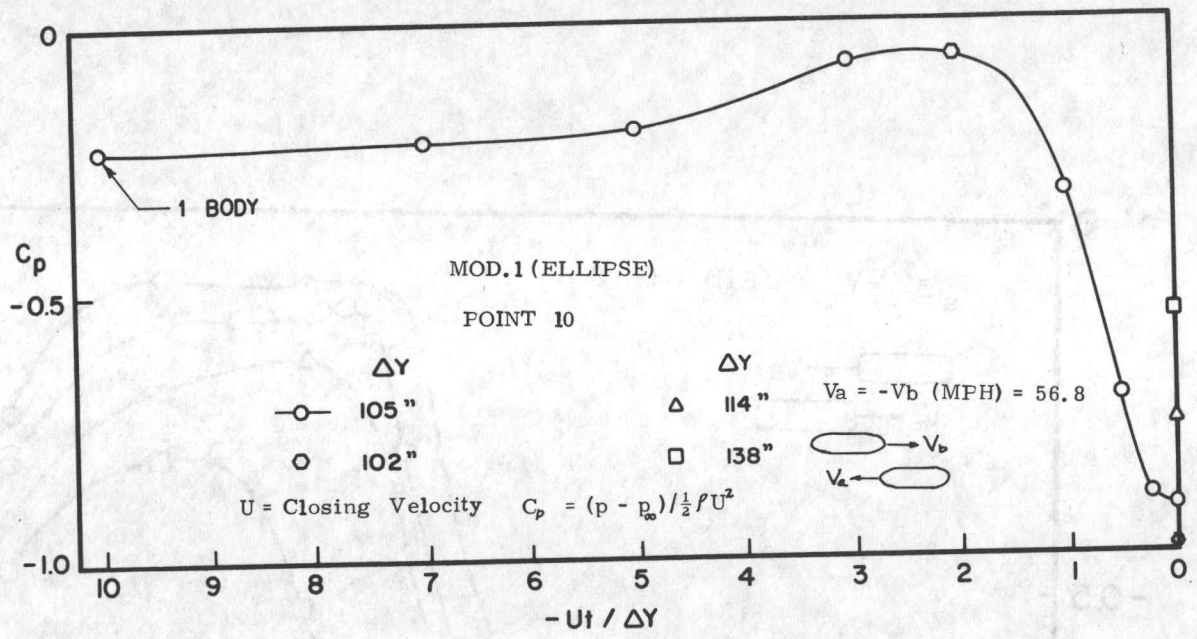

FIG. 6 PRESSURE - TIME HISTORY (BODY A)

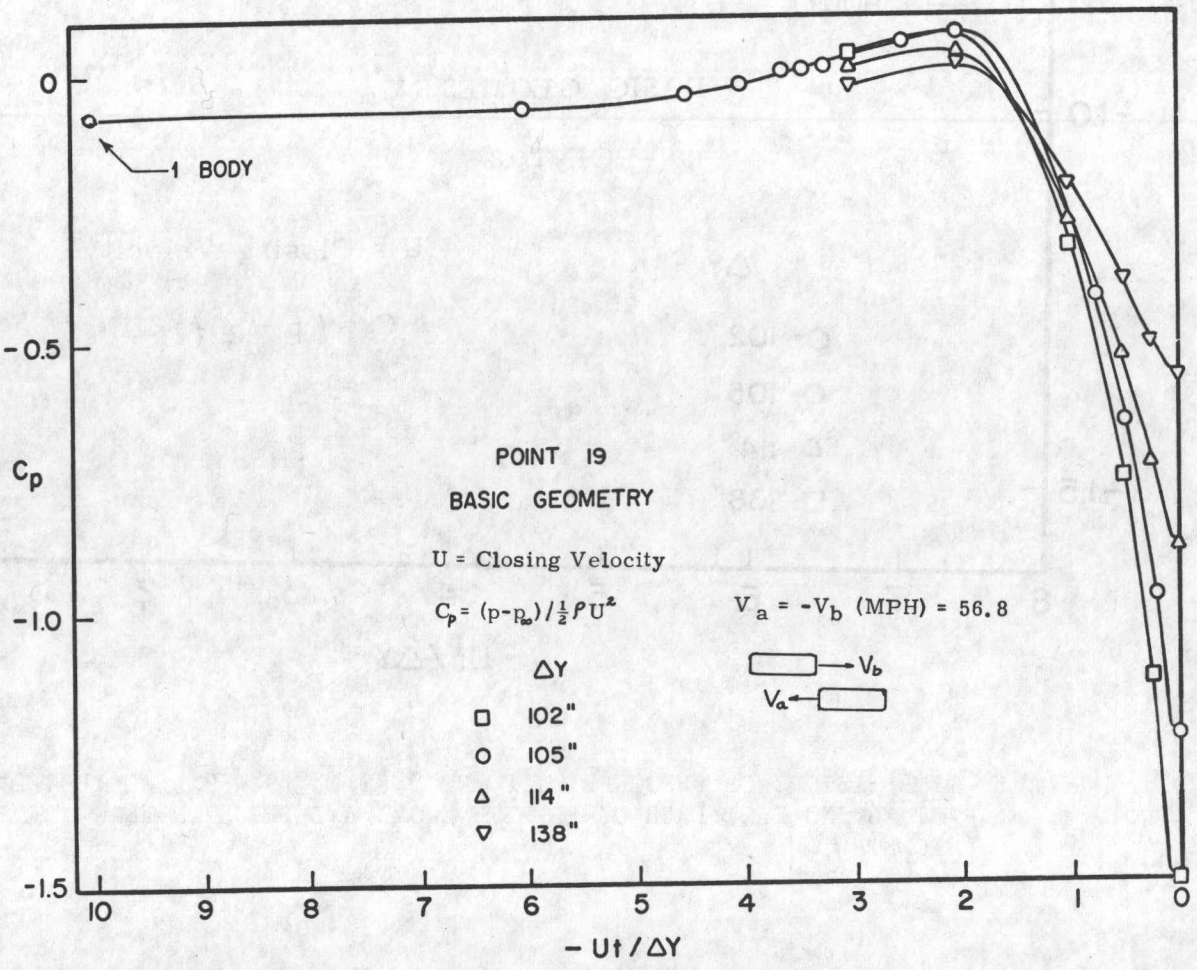

FIG. 7 PRESSURE - TIME HISTORY (BODY A)

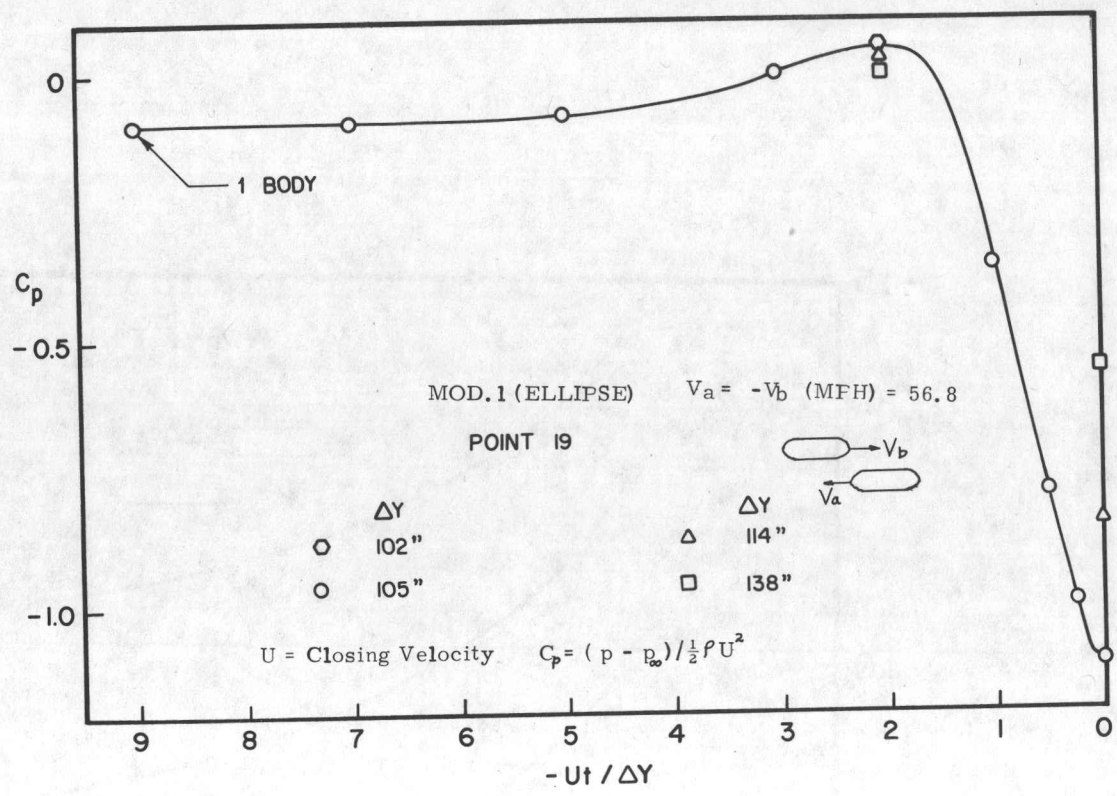

FIG. 8 PRESSURE - TIME HISTORY (BODY A)

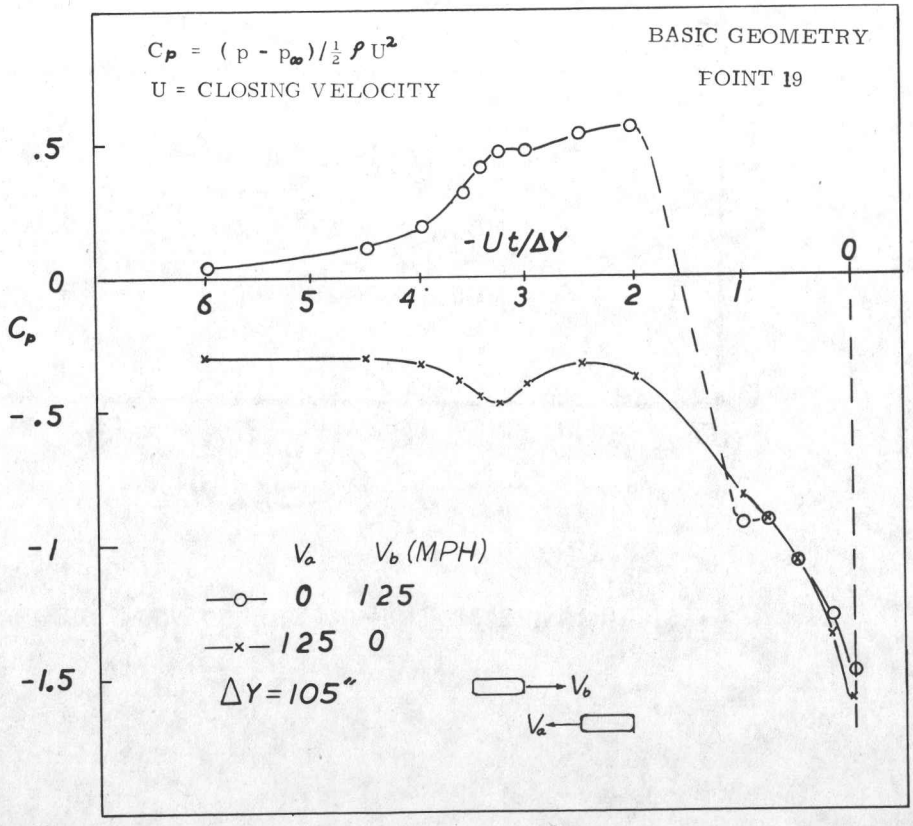

FIG. 9 PRESSURE - TIME HISTORY (BODY A)

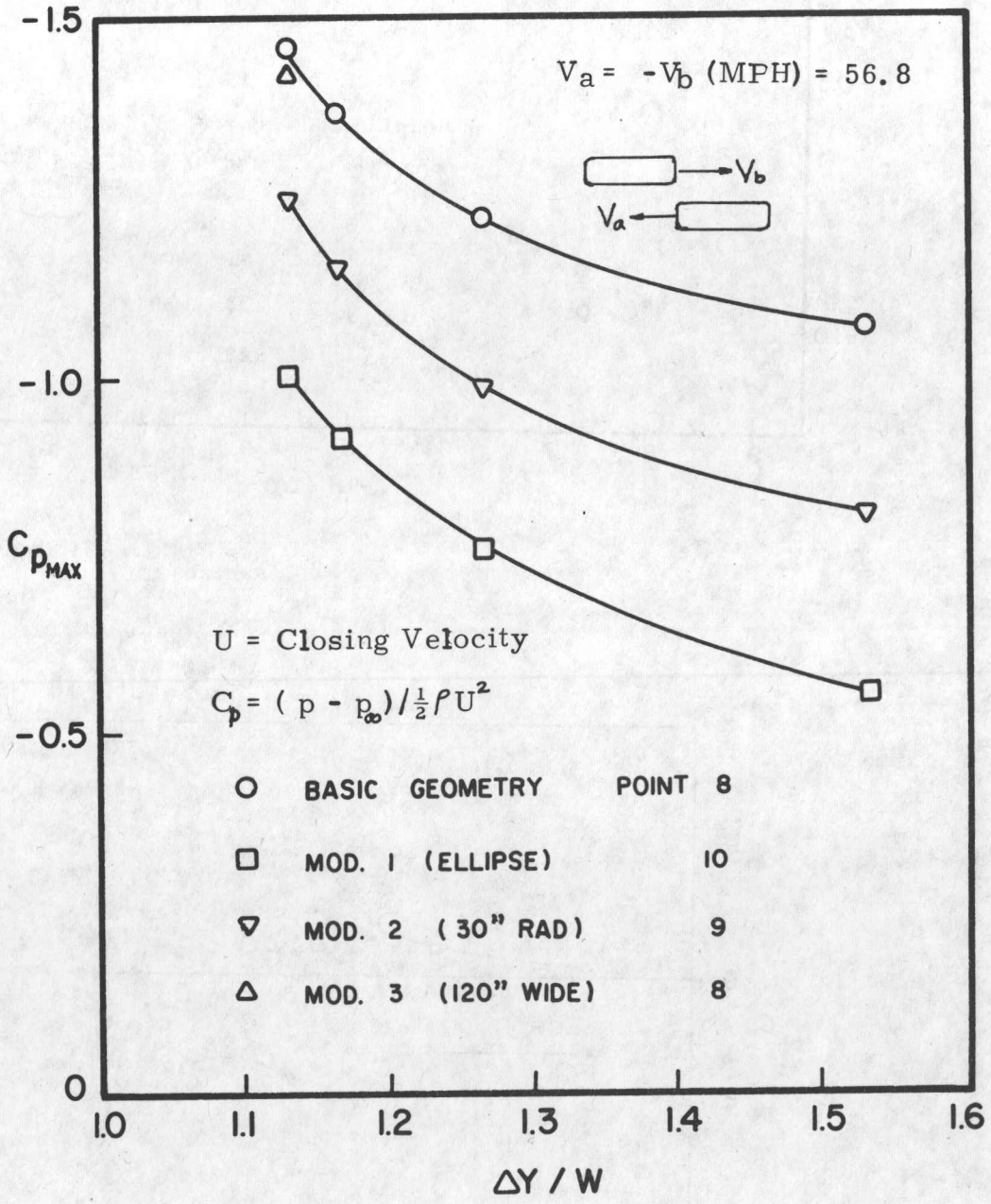

FIG. 10 VARIATION OF C_p WITH LATERAL SEPARATION (BODY A)

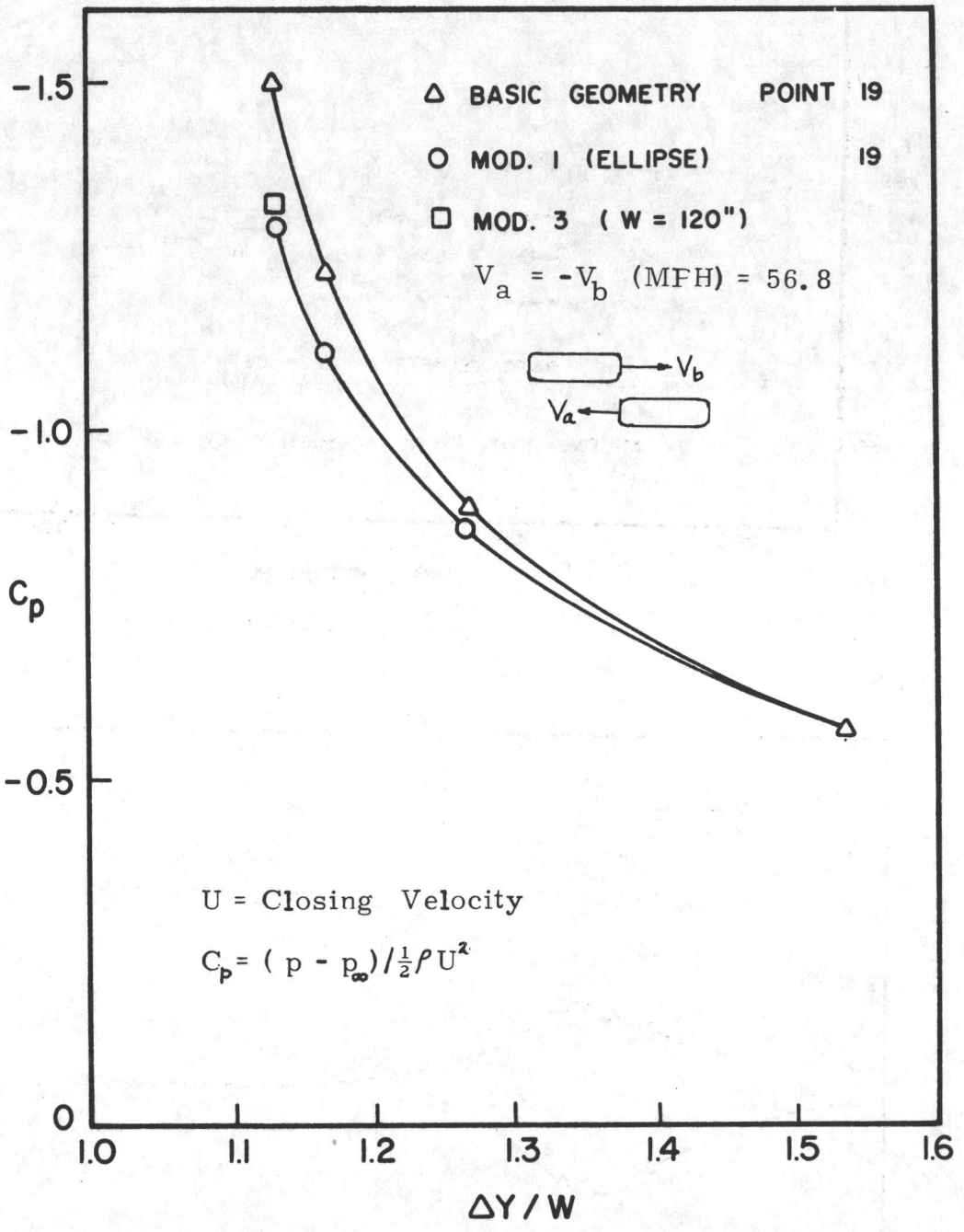

FIG. 11 VARIATION OF C_p WITH LATERAL SEPARATION (BODY A)

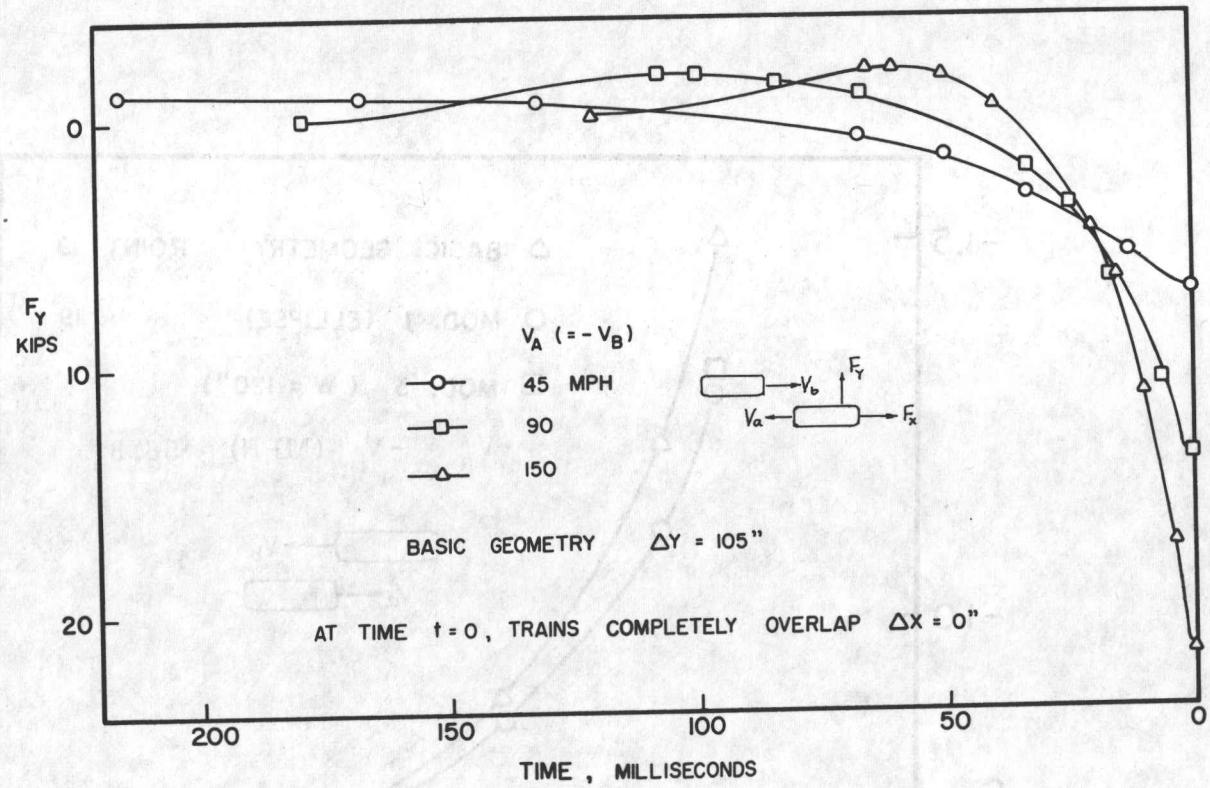

FIG. 12 FORCE - TIME HISTORY (BODY A)

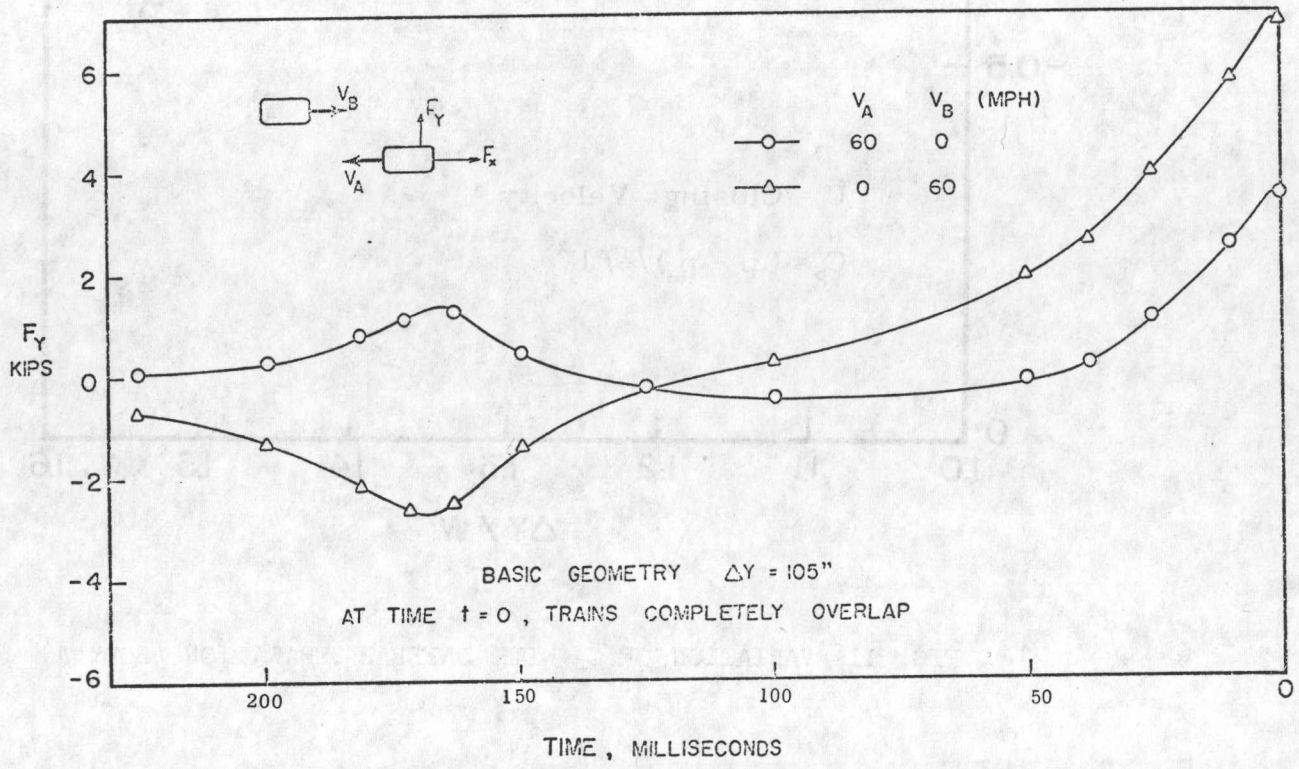

FIG. 13 FORCE - TIME HISTORY (BODY A)

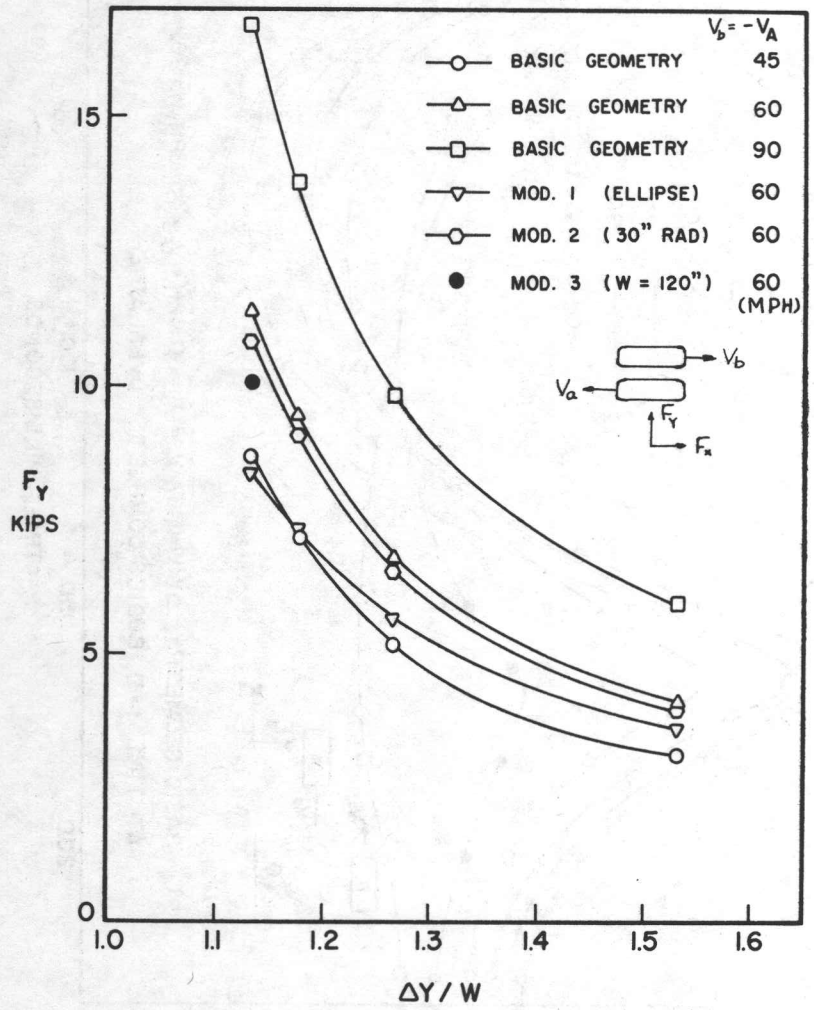

F_Y vs. LATERAL SEPARATION , $\Delta X = 0$" (BODY A)

FIG. 14 (W = TRAIN WIDTH = 90" FOR BASIC GEOMETRY , MOD. 1,2)

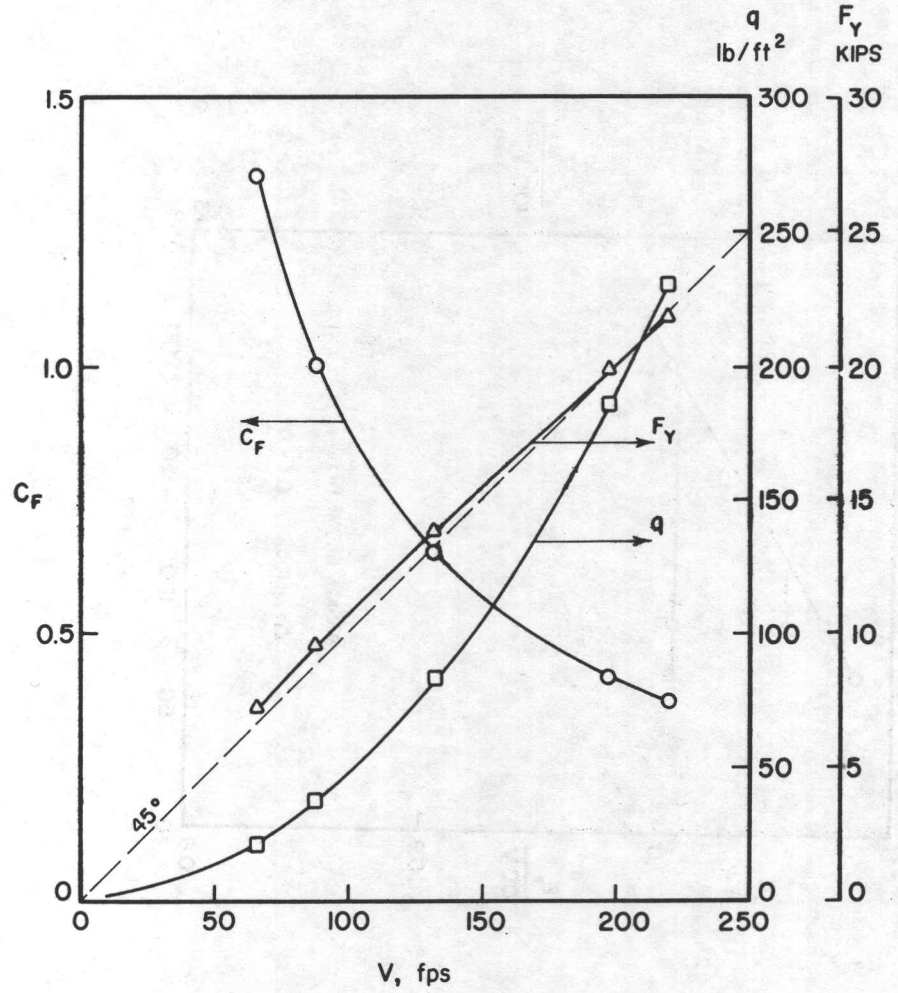

$q = \frac{1}{2} \rho (2V)^2$

$C_F = F_Y / (qS)$ where $S = 30 \times 8.5 = 255$ ft^2

BASIC GEOMETRY $\Delta Y = 105$", $\Delta X = 0$"

FIG. 15 VARIATION OF SIDE FORCE WITH VELOCITY

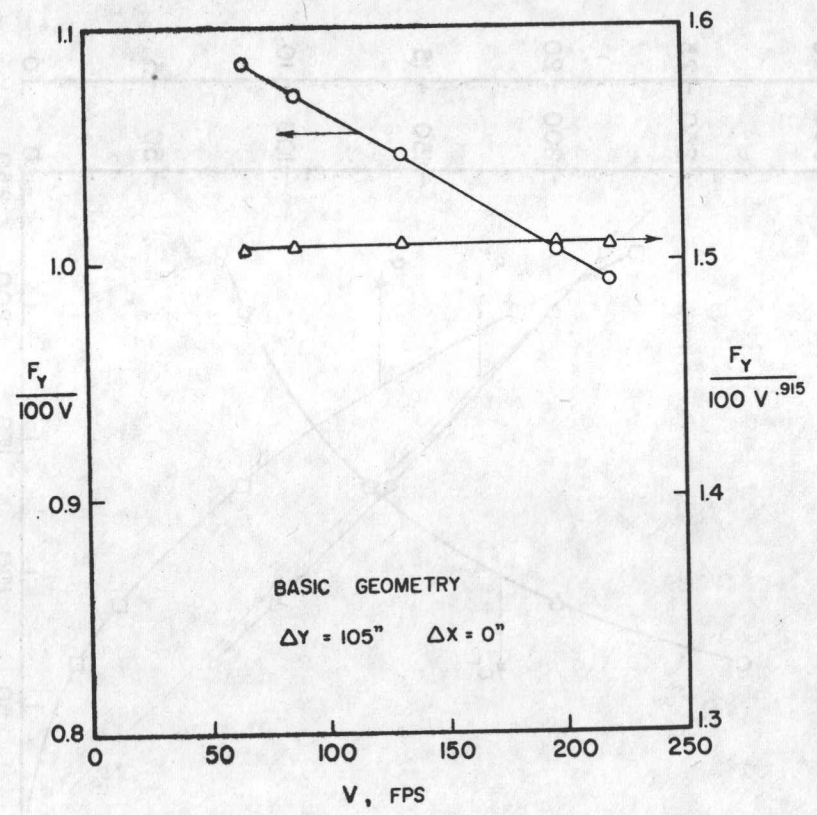

FIG. 16 VARIATION OF SIDE FORCE WITH VELOCITY

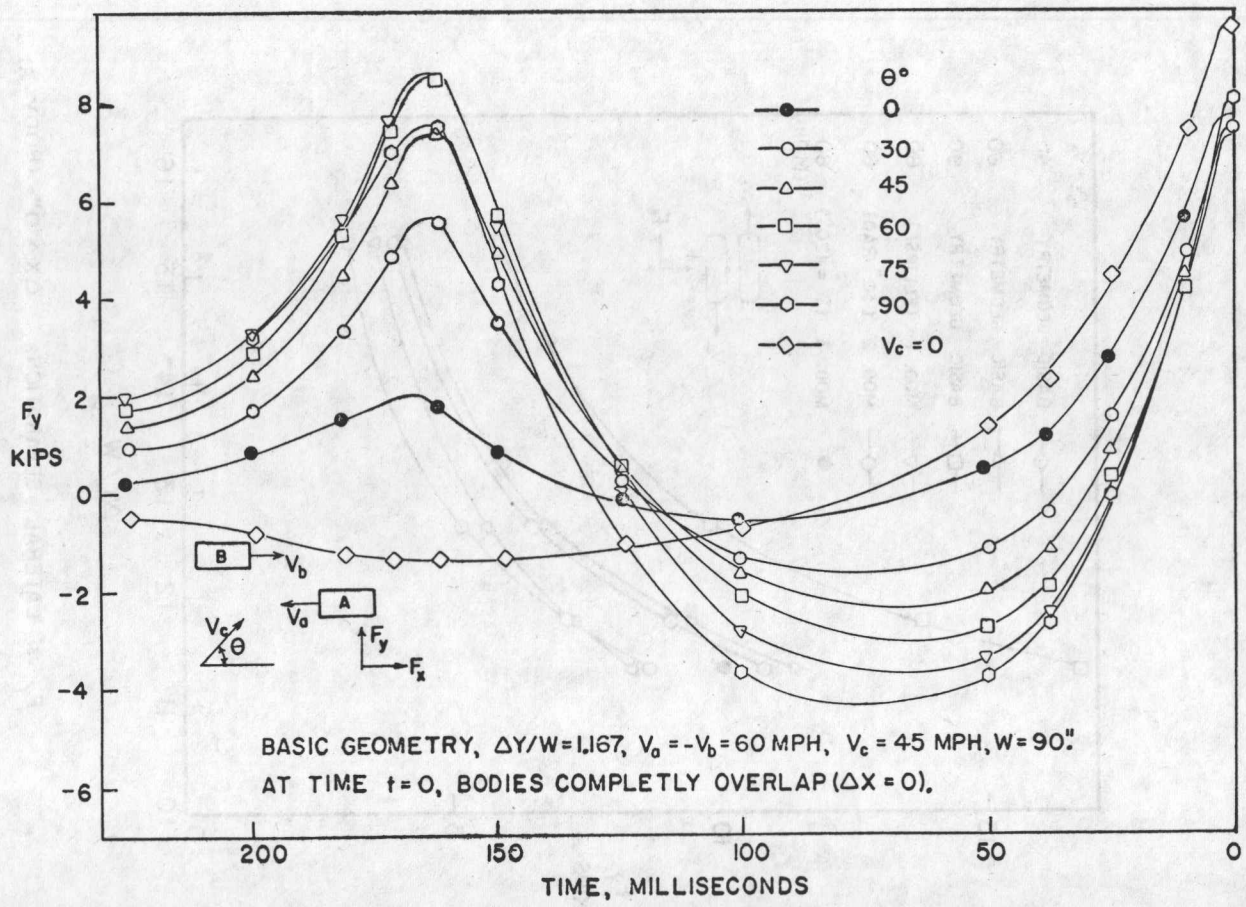

FIG. 17 FORCE - TIME HISTORY WITH CROSS WIND (BODY A)

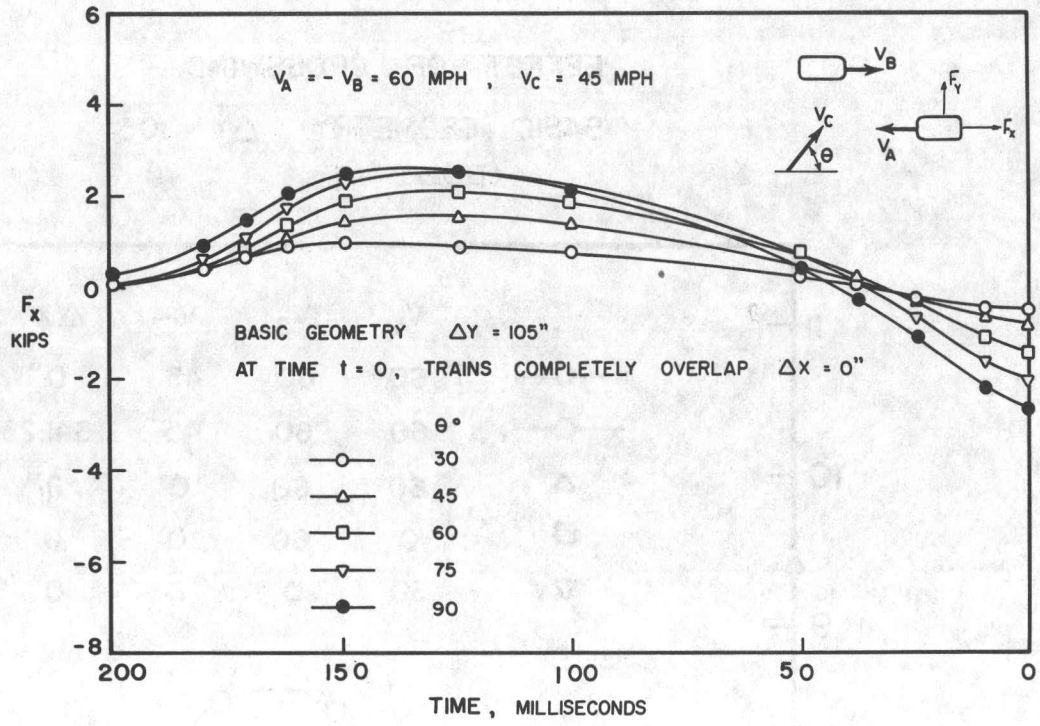

FIG. 18 FORCE - TIME HISTORY WITH CROSSWIND (BODY A)

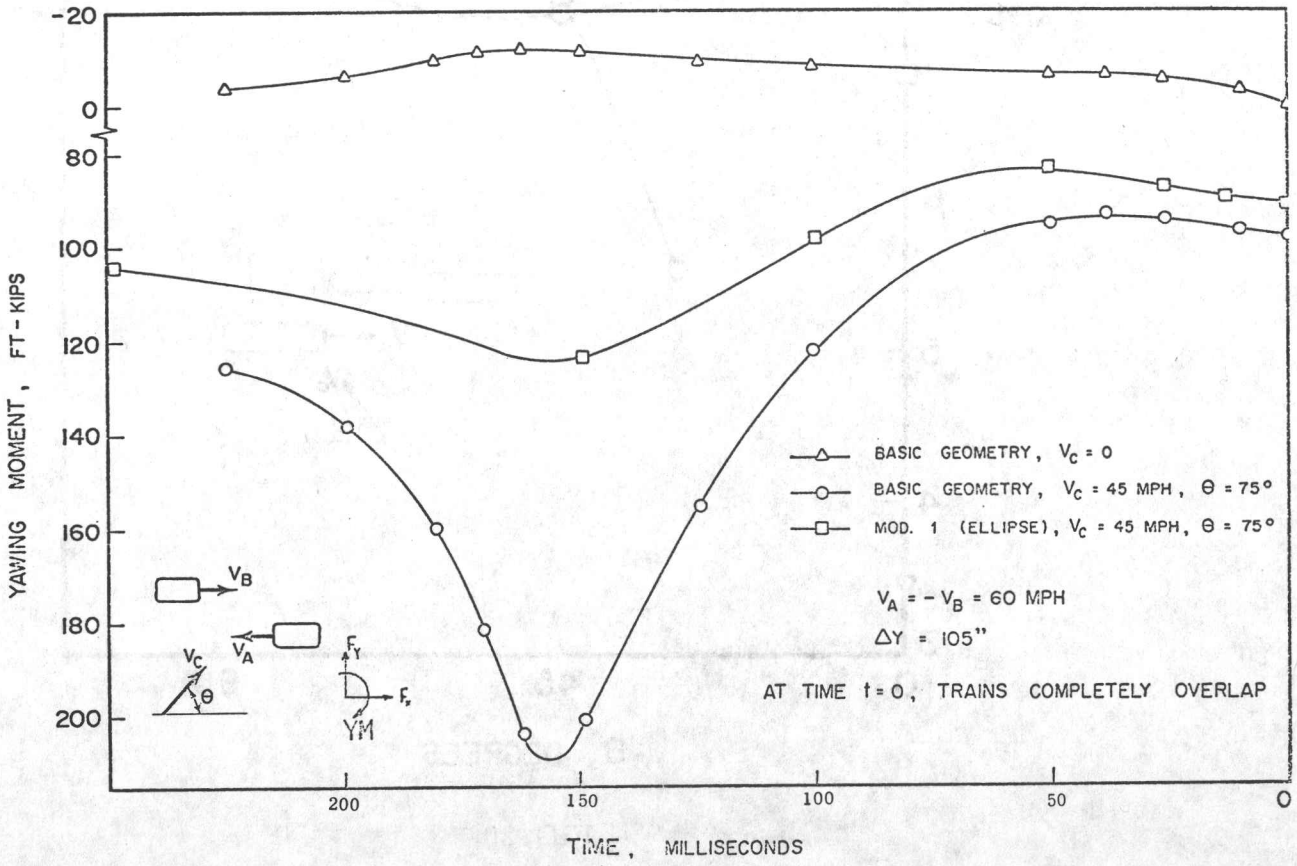

FIG. 19 YAWING MOMENT TIME HISTORY (BODY A)

EFFECT OF CROSSWIND

BASIC GEOMETRY $\Delta Y = 105"$

(BODY A)

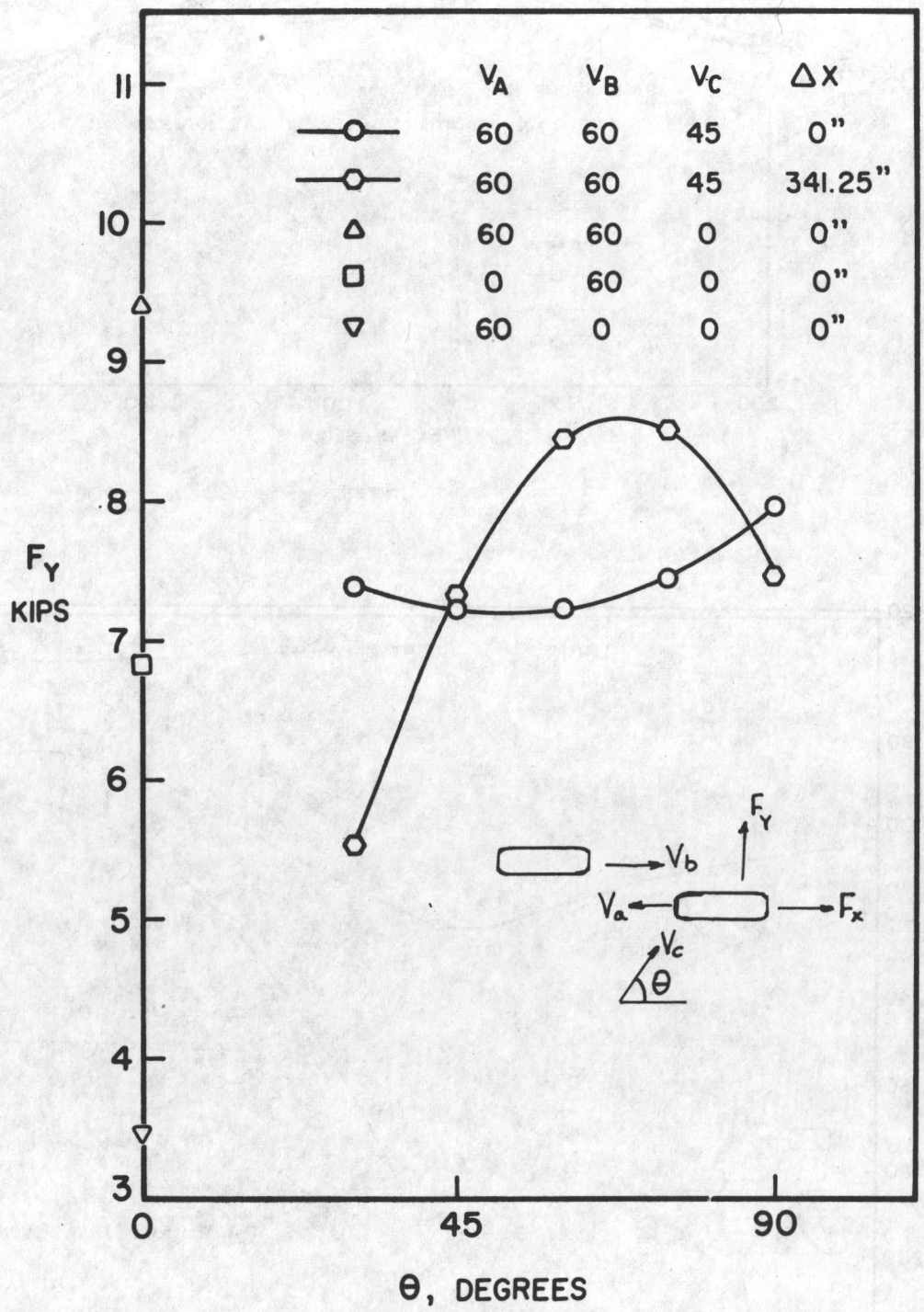

FIG. 20

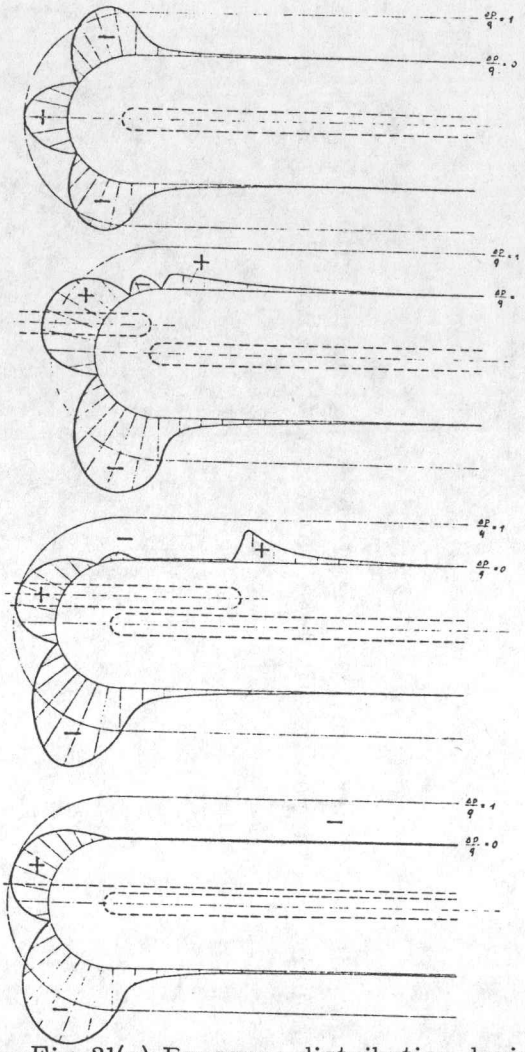

Fig. 21(a) Pressure distribution during passing at different train positions ($V_a = -V_b$) (Ref. 4)

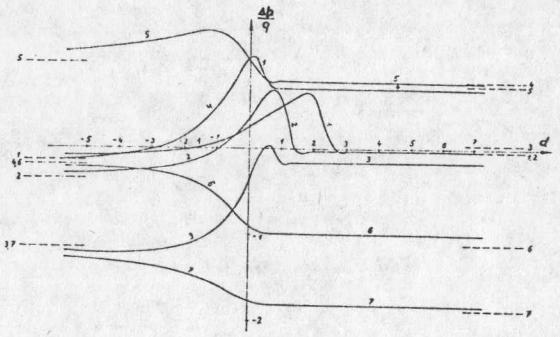

Fig. 21(b) Pressure signature during passing at various stations ($V_a = -V_b$)(Ref. 4).

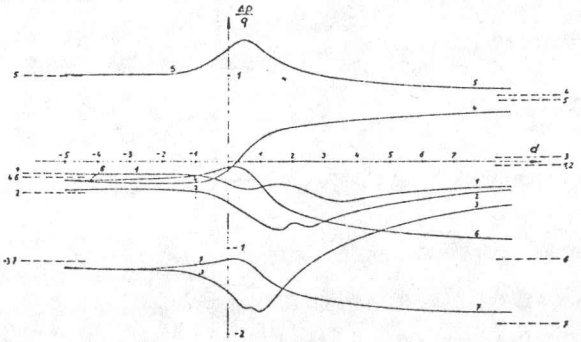

Fig. 21(c) Pressure signature during passing at different train positions of moving train ($V_b = 0$)(Ref. 4).

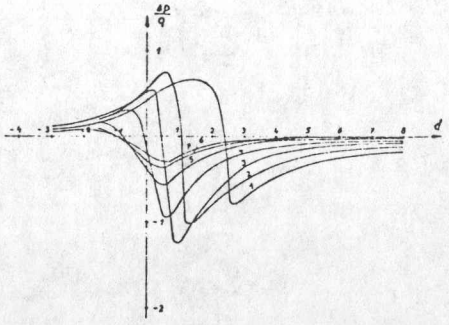

Fig. 21(d) pressure signature during passing at various stations of stationary train ($V_b = 0$) (Ref. 4)

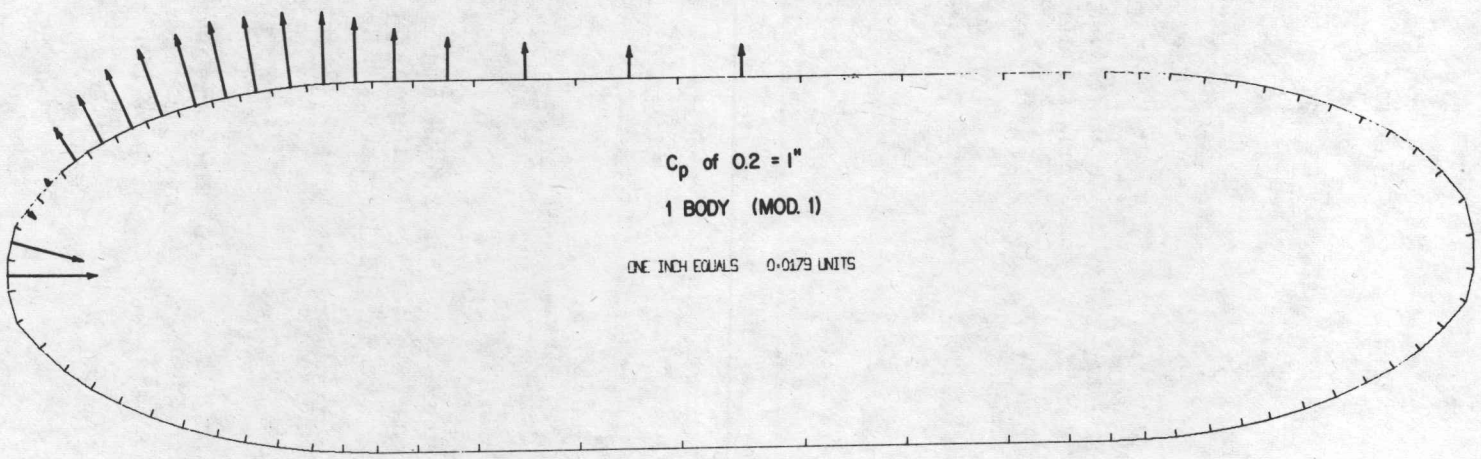

Pressure distribution on an isolated streamlined single body moving with a velocity of 56.8 mph (Reduced photographically by a factor of 2.645).

FIG. 22

Figures 23(a) to 23(j) show the pressure distribution at various time intervals on a body moving with a velocity of 56.8 mph as it approaches and passes an identical body moving in the opposite direction with the same velocity. Lateral separation between bodies is 105 inches. All the figures have been photographically reduced by a factor of 2.645.

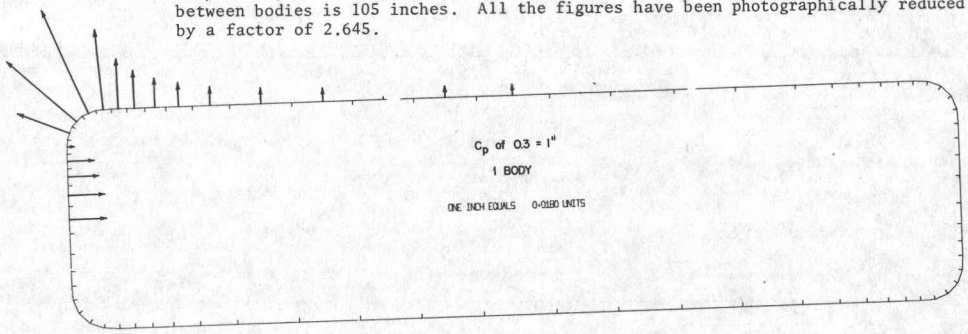

FIG. 23(a)

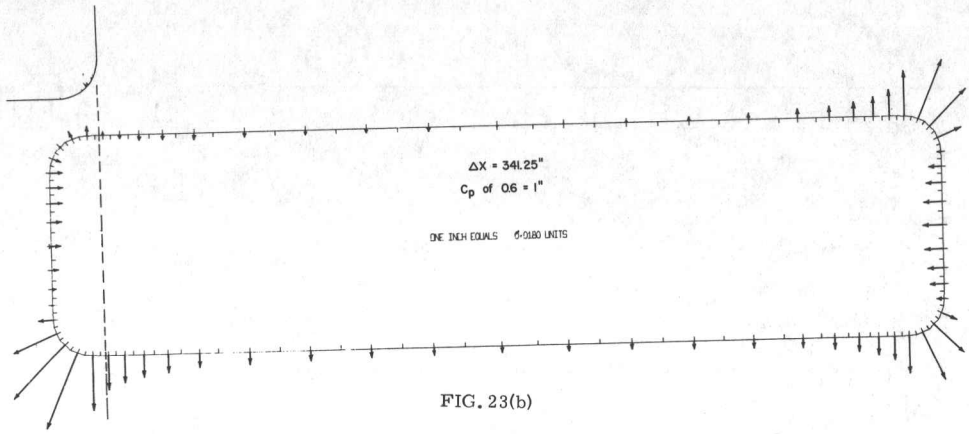

FIG. 23(b)

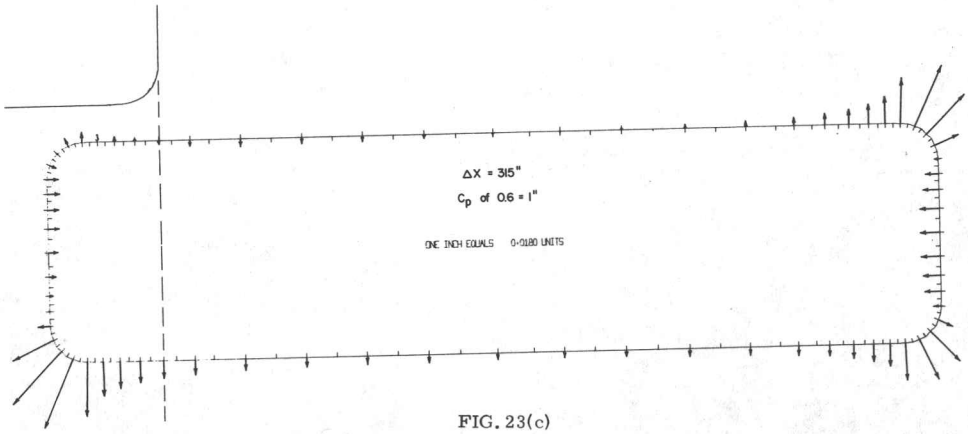

FIG. 23(c)

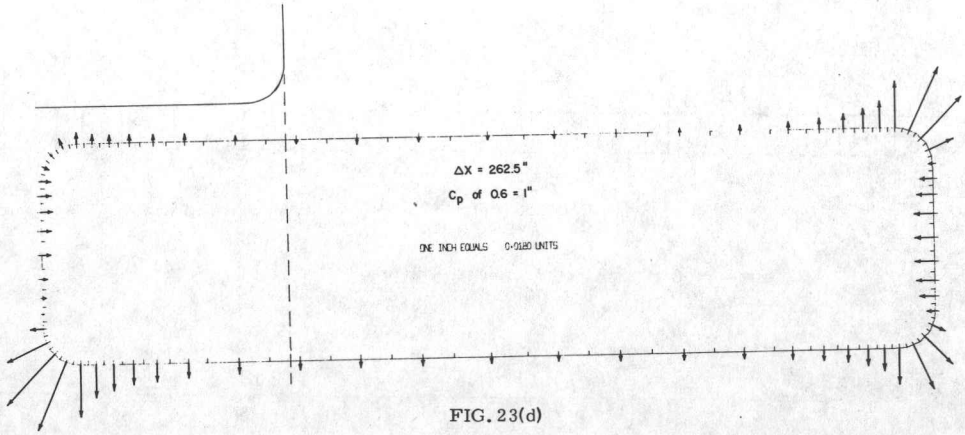

FIG. 23(d)

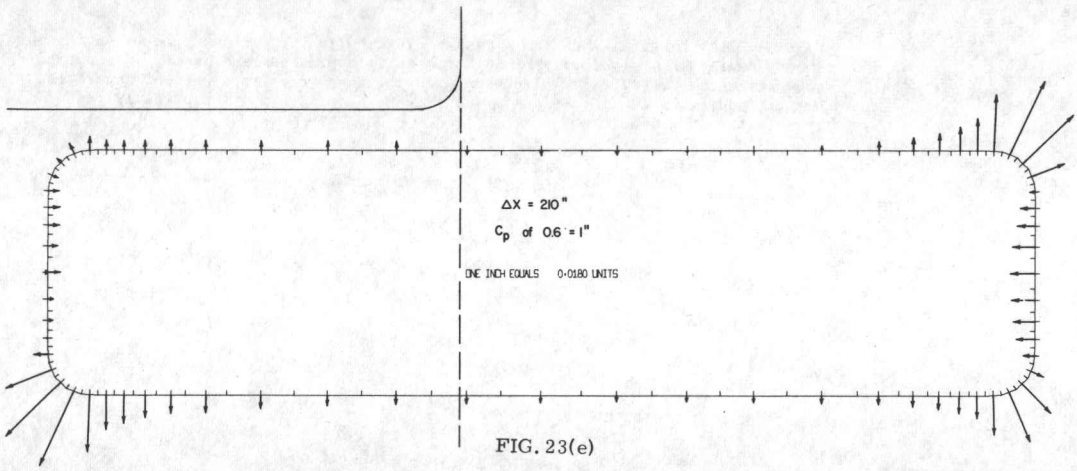

FIG. 23(e)

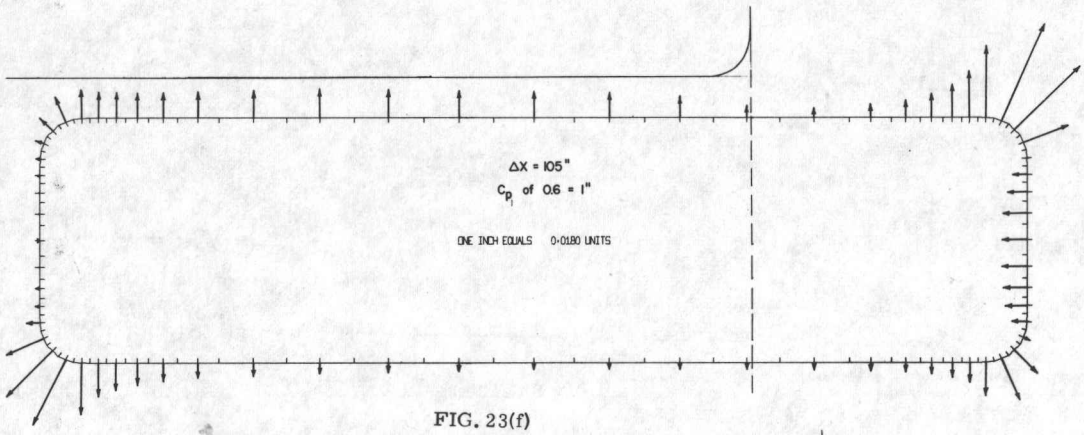

FIG. 23(f)

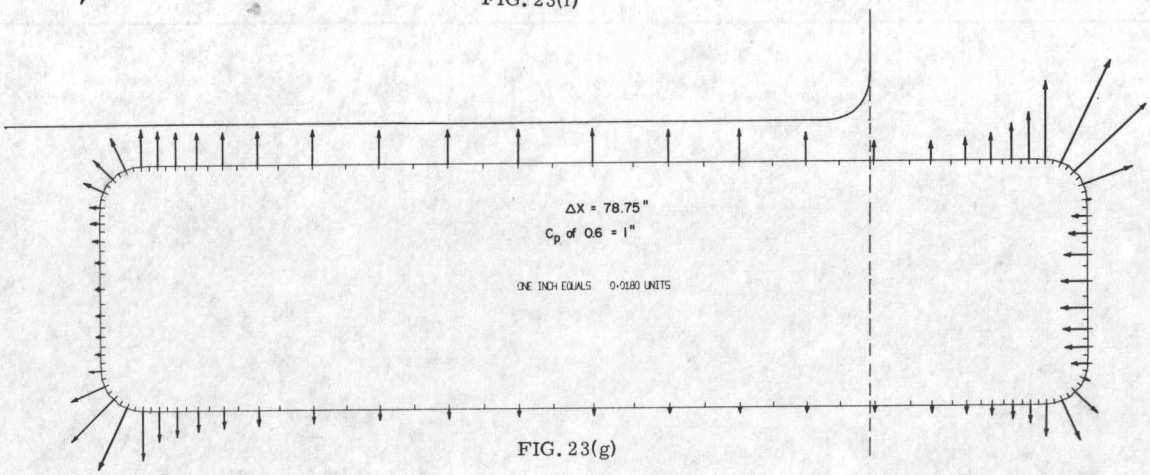

FIG. 23(g)

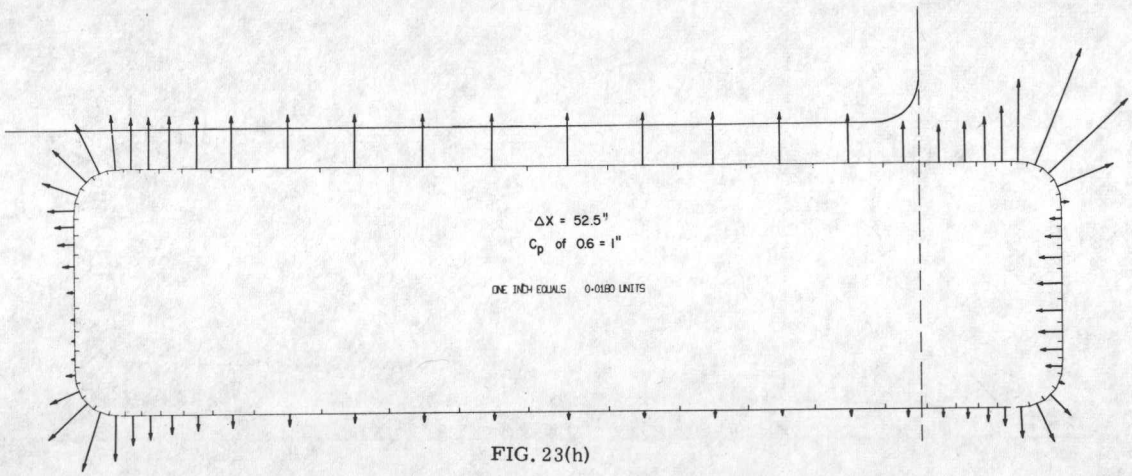

FIG. 23(h)

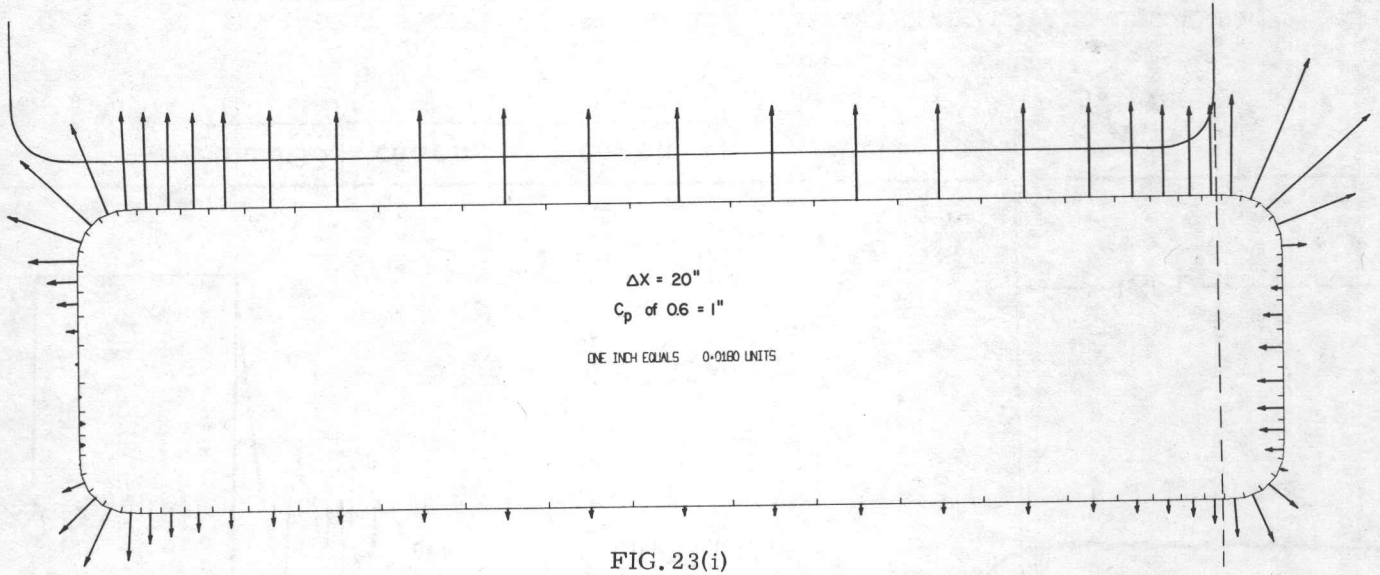

FIG. 23(i)

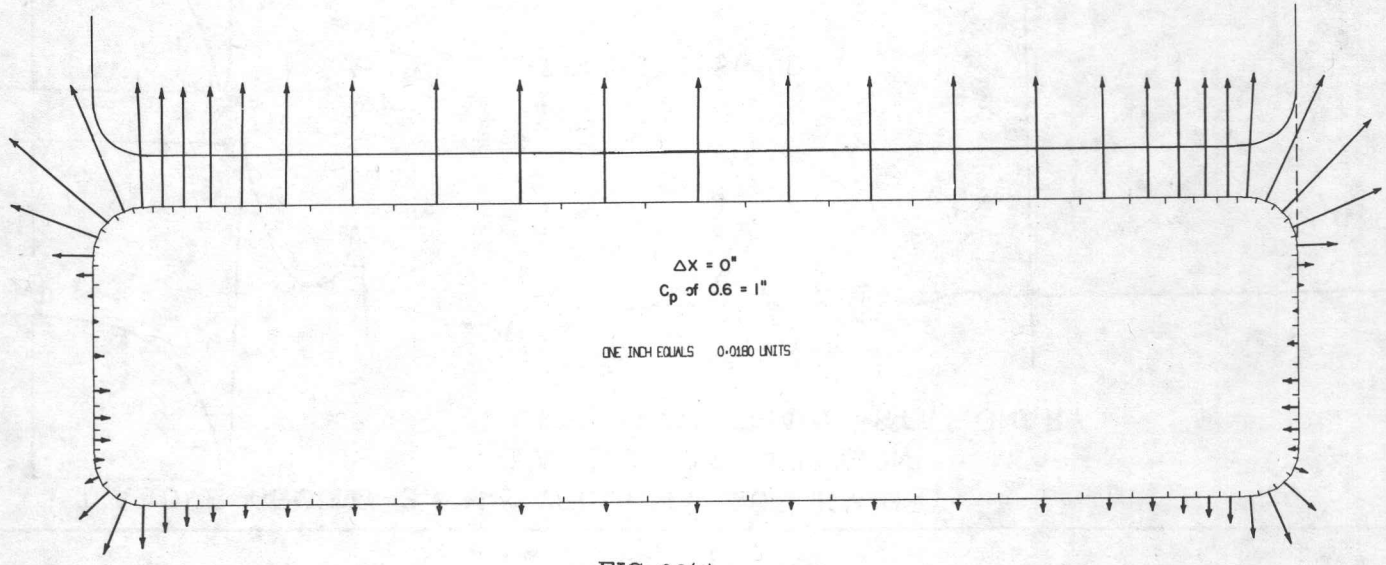

FIG. 23(j)

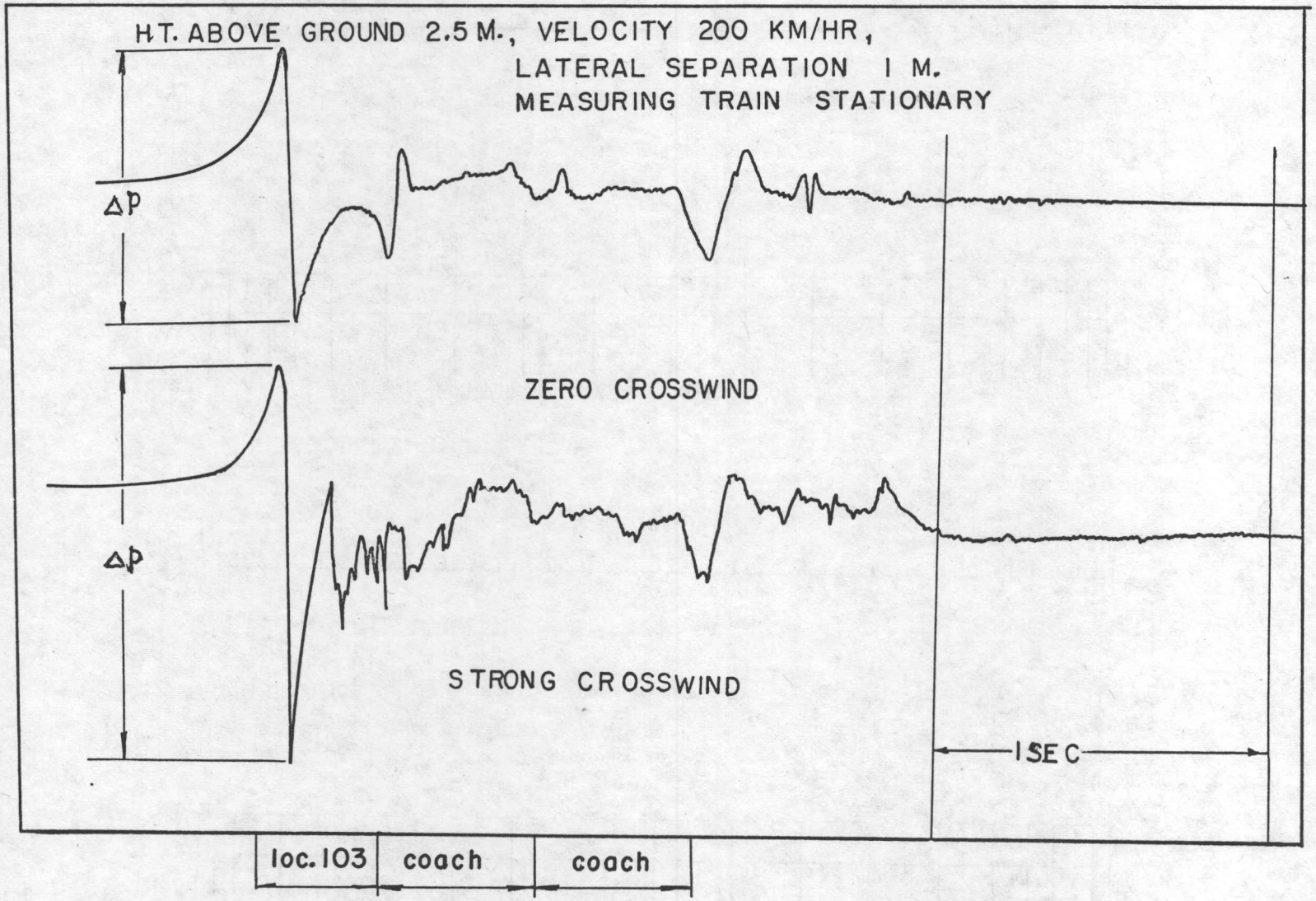

FIG. 24 COACH PRESSURE SIGNATURE RECORDED ON A STATIONARY TRAIN AS IT IS APPROACHED AND PASSED BY ANOTHER TRAIN AT 200 KM/HR (REF. 5)

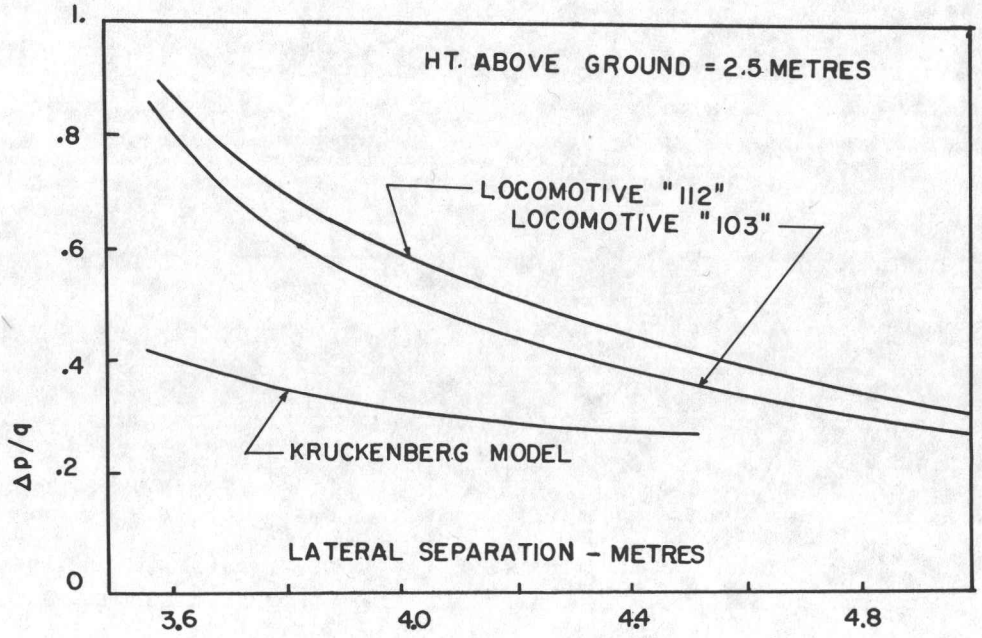

VARIATION OF PRESSURE PULSE MAGNITUDE WITH VELOCITY (FULL SCALE & WIND TUNNEL DATA)(REF. 5)

FIG. 25

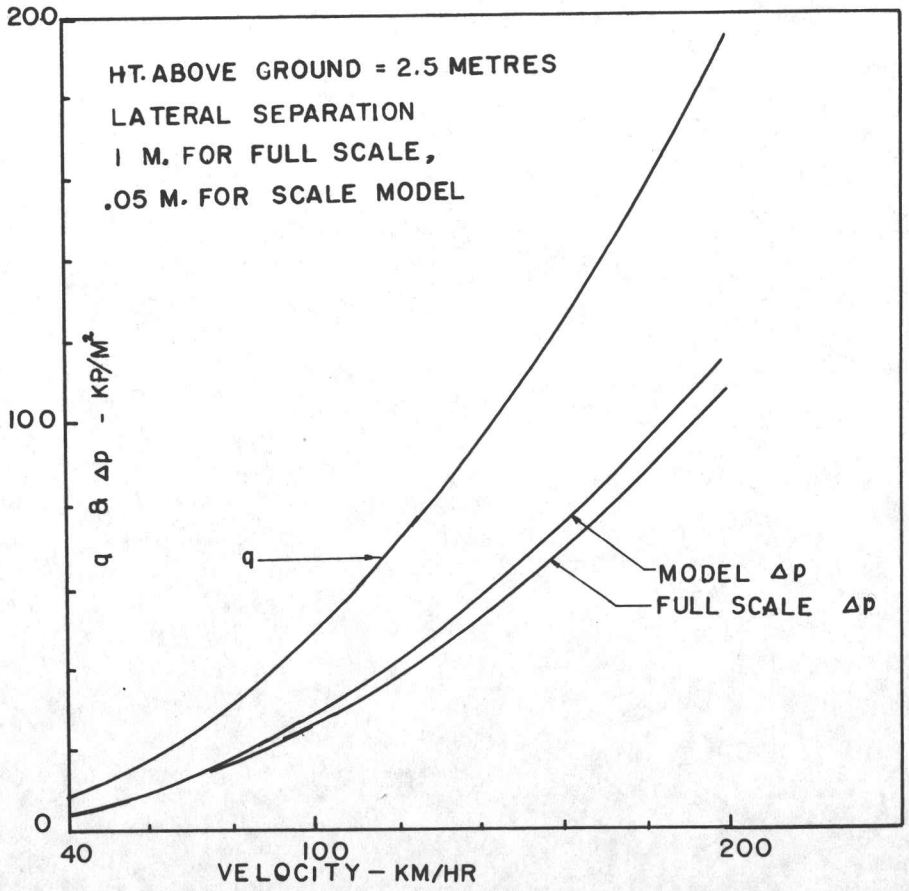

VARIATION OF PRESSURE PULSE MAGNITUDE WITH LATERAL SEPARATION (WIND TUNNEL DATA)(REF. 5)

FIG. 26

APPENDIX

DEVELOPMENT OF COMPUTATIONAL EQUATIONS

Let S be the surface of a cylinder extending from -L to L. $\sigma(s)$ is the distribution of sources of strength σ on the body. $\sigma(s)$ is assumed independent of z. s is the coordinate measured along the contour of the body. In this formulation the subscript i refers to the field point and j to the source point. Coordinates x, y, z refer to the field point and ξ, η, ζ to the source point. r is the distance from the field point to the source point.

$$r^2 = (x - \xi)^2 + (y - \eta)^2 + (z - \zeta)^2$$

Without loss of generality we can assume that z = 0. The potential at x, y, z due to the distribution of sources is

$$\varphi(x,y,z) = \iint \frac{\sigma(s)}{r}\, dS$$

or

$$\varphi(x,y,o) = \oint \sigma(s) \int_{-L}^{L} \frac{ds}{r} = \int \sigma(s) \int_{-L}^{L} \frac{d\zeta ds}{r}$$

$$\varphi(x,y,o) = \oint \sigma(s) \log \left[\frac{(\sqrt{a^2 + L^2} + L)^2}{a^2} \right] ds$$

where

$$a^2 = (x - \xi)^2 + (y - \eta)^2$$

To avoid the infinite integral that will result above as the cylinder becomes two-dimensional ($L \to \infty$) we can make use of the fact that the net source strength on the cylinder is zero, so that

$$\oint \sigma(s) \log(2L)^2 ds = 0$$

So,

$$\varphi(x,y,o) = \oint \sigma(s) \log \left(\frac{\sqrt{a^2 + L^2} + L}{2L} \right)^2 - \oint \sigma(s) \log(a^2) ds$$

Now if we let $L \to \infty$

$$\varphi(x,y,o) = -\oint \sigma(s)\, \log(a^2)ds$$

or

$$\varphi(x,y) = -\oint \sigma(s)\, \log\{(x - \xi)^2 + (y - \eta)^2\}ds$$

and

$$\frac{\partial \varphi}{\partial x} = -2\oint \sigma(s)\, \frac{(x - \xi)}{(x - \xi)^2 + (y - \eta)^2}\, ds$$

$$\frac{\partial \varphi}{\partial y} = -2\oint \sigma(s)\, \frac{(y - \eta)}{(x - \xi)^2 + (y - \eta)^2}\, ds$$

Coordinate Transformations

Consider the following coordinate transformation:

1. Body attached coordinates.
2. h is the + outward normal to the body.
3. s is + clockwise around the body.
4. j, the source point, lies on the s axis.
5. i, the field point, could be anywhere in space.
6. α is measured from + x to s.

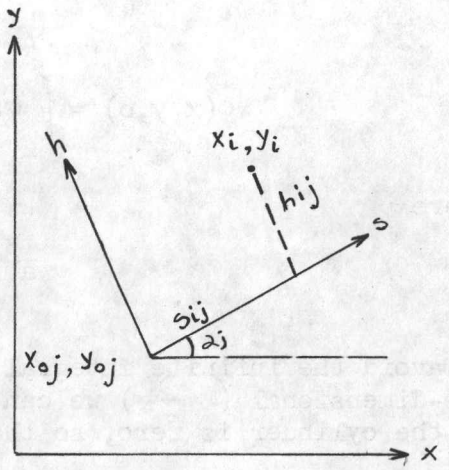

From the figure, it is seen that

$$x_i = x_{oj} + (s_{ij}\cos\alpha_j - h_{ij}\sin\alpha_j)$$

$$y_i = y_{oj} + (s_{ij}\sin\alpha_j + h_{ij}\cos\alpha_j)$$

for the source point, $h_{ij} = 0$, $s_{ij} = s$

$$\xi = x_{oj} + s\cos\alpha_j$$

$$\eta = y_{oj} + s\sin\alpha_j$$

$$x_i - \xi = (s_{ij} - s)\cos\alpha_j - h_{ij}\sin\alpha_j$$

$$y_i - \eta = (s_{ij} - s)\sin\alpha_j + h_{ij}\cos\alpha_j$$

$$(x_i - \xi)^2 + (y_i - \eta)^2 = (s_{ij} - s)^2(\cos^2\alpha_j + \sin^2\alpha_j)$$

$$+ h_{ij}^2(\sin^2\alpha_j + \cos^2\alpha_j)$$

$$+ 2h_{ij}\sin\alpha_j\cos\alpha_j - 2h_{ij}\sin\alpha_j\cos\alpha_j$$

$$= (s_{ij} - s)^2 + h_{ij}^2$$

$$\varphi(x, y) = -\oint \sigma(s)\log[(s_{ij} - s)^2 + h_{ij}^2]ds$$

$$\frac{\partial\varphi}{\partial x} = -2\sigma(s)\frac{(s_{ij} - s)\cos\alpha_j - h_{ij}\sin\alpha_j}{(s_{ij} - s)^2 + h_{ij}^2}ds$$

$$\frac{\partial\varphi}{\partial y} = -2\sigma(s)\frac{(s_{ij} - s)\sin\alpha_j + h_{ij}\cos\alpha_j}{(s_{ij} - s)^2 + h_{ij}^2}$$

Before proceeding further with the integration, we have to get expressions for s_{ij} and h_{ij} in terms which can be calculated. We can write:

$$s = (x - x_o)\cos\alpha + (y - y_o)\sin\alpha$$

$$h = -(x - x_o)\sin\alpha + (y - y_o)\cos\alpha$$

If we write

$$s_o = -x_o\cos\alpha - y_o\sin\alpha$$

$$h_o = x_o\sin\alpha - y_o\cos\alpha$$

then

$$s = s_o + x\cos\alpha + y\sin\alpha$$

$$h = h_o - x\sin\alpha + y\cos\alpha$$

For a specific point, and s_{oj} and h_{oj} can be calculated from

$$s_{oj} = s_j - x_j\cos\alpha_j - y_j\sin\alpha_j$$

$$h_{oj} = h_j + x_j\sin\alpha_j - y_j\cos\alpha_j \qquad \text{(Note: } h_j = 0\text{)}$$

and

$$s_{ij} = s_{oj} + x_i\cos\alpha_j + y_i\sin\alpha_j$$

$$h_{ij} = h_{oj} + x_i\sin\alpha_j - y_i\cos\alpha_j$$

Integration for φ and φ Derivatives

At this point we can write the integral as a sum over n segments, obtaining

$$\varphi_i(x, y) = -\sum_{j=1}^{n}\int_{s_j}^{s_{j+1}} \sigma_j(s)\log\{(s_{ij} - s)^2 + h_{ij}^2\}ds$$

$$\frac{\partial\varphi_i}{\partial x} = -2\sum_{j=1}^{n}\int_{s_j}^{s_{j+1}} \sigma_j(s)\,\frac{(s_{ij} - s)\cos\alpha_j - h_{ij}\sin\alpha_j}{(s_{ij} - s)^2 + h_{ij}^2}\,ds$$

$$\frac{\partial\varphi_i}{\partial y} = -2\sum_{j=1}^{n}\int_{s_j}^{s_{j+1}} \sigma_j(s)\,\frac{(s_{ij} - s)\sin\alpha_j + h_{ij}\cos\alpha_j}{(s_{ij} - s)^2 + h_{ij}^2}\,ds$$

By making suitable assumptions for the distribution of σ over the element we can integrate the above equations.

1. σ is constant over each element but varies from element to element.

2. σ varies linearly over each element as well as varying from element to element.

If we assume σ constant over each element the equations become

$$\varphi_i(x,y) = -\sum_{j=1}^{n} \sigma_j \int_{s_j}^{s_{j+1}} \log\{(s_{ij} - s)^2 + h_{ij}^2\} ds$$

$$\frac{\partial \varphi_i}{\partial x} = -2 \sum_{j=1}^{n} \sigma_j \int_{s_j}^{s_{j+1}} \frac{(s_{ij} - s)\cos\alpha_j - h_{ij}\sin\alpha_j}{(s_{ij} - s)^2 + h_{ij}^2} ds$$

$$\frac{\partial \varphi_i}{\partial y} = -2 \sum_{j=1}^{n} \sigma_j \int_{s_j}^{s_{j+1}} \frac{(s_{ij} - s)\sin\alpha_j + h_{ij}\cos\alpha_j}{(s_{ij} - s)^2 + h_{ij}^2} ds$$

In these two equations we have three different integrals of the form

$$\int \log(a^2 + x^2) dx = x \log(a^2 + x^2) - 2x + 2|a| \tan^{-1} \frac{x}{a}$$

$$\int \frac{dx}{a^2 + x^2} = \frac{a}{|a|} \tan^{-1} \frac{x}{|a|}$$

$$\int \frac{x}{a^2 + x^2} dx = \frac{1}{2} \log(x^2 + a^2)$$

If we assume σ to vary linearly within each element,

$$\sigma_j(s) = \sigma_j + \frac{(s - s_{m_j})}{(s_{m_{j+1}} - s_{m_{j-1}})} (\sigma_{j+1} - \sigma_{j-1})$$

where subscript m stands for the mid-point of the element.

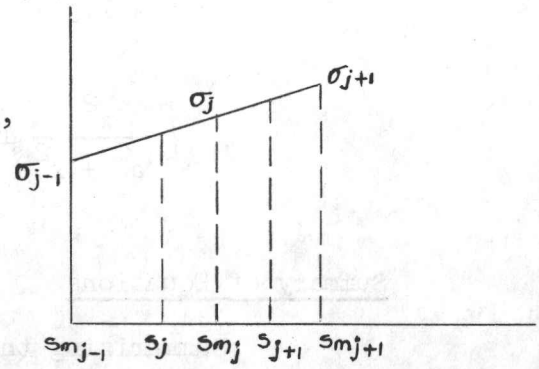

$$\varphi_i(x,y) = -\sum_{j=1}^{n}\Bigg[\sigma_j\int_{s_j}^{s_{j+1}}\log\{(s_{ij}-s)+h_{ij}\}ds$$

$$+\frac{\sigma_{j+1}-\sigma_{j-1}}{s_{m_{j+1}}-s_{m_{j-1}}}\int_{s_j}^{s_{j+1}}(s-s_{m_j})\log\{(s_{ij}-s)^2+h_{ij}^2\}ds\Bigg]$$

$$\frac{\partial\varphi_i}{\partial x} = -2\sum_{j=1}^{n}\Bigg[\sigma_j\int_{s_j}^{s_{j+1}}\frac{(s_{ij}-s)\cos\alpha_j - h_{ij}\sin\alpha_j}{(s_{ij}-s)^2+h_{ij}^2}ds$$

$$+\frac{\sigma_{j+1}-\sigma_{j-1}}{s_{m_{j+1}}-s_{m_{j-1}}}\int_{s_j}^{s_{j+1}}(s-s_{m_j})\frac{(s_{ij}-s)\cos\alpha_j - h_{ij}\sin\alpha_j}{(s_{ij}-s)^2+h_{ij}^2}ds\Bigg]$$

$$\frac{\partial\varphi_i}{\partial y} = -2\sum_{j=1}^{n}\Bigg[\sigma_j\int_{s_j}^{s_{j+1}}\frac{(s_{ij}-s)\sin\alpha_j + h_{ij}\cos\alpha_j}{(s_{ij}-s)^2+h_{ij}^2}ds$$

$$+\frac{\sigma_{j+1}-\sigma_{j-1}}{s_{m_{j+1}}-s_{m_{j-1}}}\int_{s_j}^{s_{j+1}}(s-s_{m_j})\frac{(s_{ij}-s)\sin\alpha_j + h_{ij}\cos\alpha_j}{(s_{ij}-s)^2+h_{ij}^2}ds\Bigg]$$

The only new integrals that appear due to the second assumption are:

$$\int x\log(a^2+x^2)dx = \frac{1}{2}(x^2+a^2)[\log(x^2+a^2)-1]$$

$$\int\frac{x^2}{a^2+x^2}dx = x - |a|\tan^{-1}\frac{x}{|a|}$$

Summary of Equations

Summarizing the various terms we have the following:

$$I^o = \int_{s_j}^{s_{j+1}}\log\{(s-s_{ij})^2+h_{ij}^2\}ds$$

$$I^1 = \int_{s_j}^{s_{j+1}} (s - s_{m_j}) \log\{(s - s_{ij})^2 + h_{ij}^2\} ds$$

$$J^o = \int_{s_j}^{s_{j+1}} \frac{h_{ij}}{(s - s_{ij})^2 + h_{ij}^2} ds$$

$$J^1 = \int_{s_j}^{s_{j+1}} (s - s_{m_j}) \frac{h_{ij}}{(s - s_{ij})^2 + h_{ij}^2} ds$$

$$K^o = \int_{s_j}^{s_{j+1}} \frac{(s - s_{ij})}{(s - s_{ij}) + h_{ij}} ds$$

$$K^1 = \int_{s_j}^{s_{j+1}} \frac{(s - s_{m_j})(s - s_{ij})}{(s - s_{ij})^2 + h_{ij}^2} ds$$

$$\varphi_i = -\sum_{j=1}^{n} \sigma_j I^o - \Delta s_j (\sigma_{j+1} - \sigma_{j-1}) I^1$$

$$\frac{\partial \varphi_i}{\partial x} = 2 \sum_{j=1}^{n} \sigma_j (J^o \sin\alpha_j + K^o \cos\alpha_j)$$

$$+ \Delta s_j (\sigma_{j+1} - \sigma_{j-1})(J^1 \sin\alpha_j + K^1 \cos\alpha_j)$$

$$\frac{\partial \varphi_i}{\partial y} = 2 \sum \sigma_j (-J^o \cos\alpha_j + K^o \sin\alpha_j)$$

$$+ \Delta s_j (\sigma_{j+1} - \sigma_{j-1})(-J^1 \cos\alpha_j + K^1 \sin\alpha_j)$$

Thus it is seen that the equations are of the form:

$$\frac{\partial \varphi_i}{\partial x} = \sum_{j=1}^{n} \sigma_j X_{ij}$$

$$\frac{\partial \varphi_i}{\partial y} = \sum_{j=1}^{n} \sigma_j Y_{ij}$$

$$\varphi_i = \sum_{j=1}^{n} \sigma_j Z_{ij}$$

where X_{ij}, Y_{ij} and Z_{ij} are the matrices formed by the various integrals. They can be calculated using the geometry of the configuration. $\partial\varphi/\partial x$ and $\partial\varphi/\partial y$ are the u and v components of velocity. The normal and tangential components are given by:

$$\frac{\partial \varphi_i}{\partial n} = \sum_{j=1}^{n} \sigma_j [- X_{ij} \sin\alpha_i + Y_{ij} \cos\alpha_i]$$

$$\frac{\partial \varphi_i}{\partial s} = \sum_{j=1}^{n} \sigma_j [X_{ij} \cos\alpha_i + Y_{ij} \sin\alpha_i]$$

The solution is obtained when the proper boundary condition is imposed on the normal derivative at the surface to get a set of n algebraic linear equations in the n unknown σ_j's.

UTIAS Report No. 185

Institute for Aerospace Studies, University of Toronto

AERODYNAMIC INTERFERENCE OF HIGH SPEED GROUND VEHICLES

Johnston, G. W., Seshagiri, B. V., Ellis, N. D. 34 pages 26 figures 5 tables

1. Aerodynamic Interference 2. Unsteady Potential Flow 3. Ground Vehicles
4. Cross Wind Interference 5. Impulsive Loadings

I. Johnston, G. W., Seshagiri, B. V., Ellis, N. D. II. UTIAS Report No. 185

A two-dimensional, incompressible, potential flow solution based on A.M.O. Smith's method has been developed capable of predicting the unsteady interference pressure loadings on either moving or stationary bodies of arbitrary shape due to the passage of a second body. The pressure distribution has been suitably integrated to yield overall forces (side and axial) and moments (rolling and yawing). Effects of crosswinds of arbitrary magnitude and direction can be accurately included. The results of a wide range of computations using different body configurations are presented and analysed. The studies carried out indicate that substantial aerodynamic interference loads may be expected under real train passage conditions. These loads, impulsive in nature, depend on the type of body geometry, the lateral spacing between the bodies, and the closing velocity. In general, streamlining greatly reduces these loads, as does increased lateral spacing. Crosswinds significantly alter the predicted loadings, tending to increase them. The interference loading induced on a stationary vehicle when passed by a moving vehicle appears to impose the most critical design loads, for conditions of zero crosswind. Velocity scaling of the interference loadings presents inherent difficulties due to the basic unsteady nature of the problem. No simple and generally applicable velocity scaling laws are expected to emerge for this problem, however over limited ranges of conditions "ad hoc" velocity rules (trends) can certainly be obtained. The basic unsteady nature of this problem also greatly complicates experimental studies. The usual steady state wind tunnel methods will generally be inadequate; preference is strongly indicated for true unsteady motion simulation at reduced physical scale.

Available copies of this report are limited. Return this card to UTIAS, if you require a copy.

UTIAS Report No. 185

Institute for Aerospace Studies, University of Toronto

AERODYNAMIC INTERFERENCE OF HIGH SPEED GROUND VEHICLES

Johnston, G. W., Seshagiri, B. V., Ellis, N. D. 34 pages 26 figures 5 tables

1. Aerodynamic Interference 2. Unsteady Potential Flow 3. Ground Vehicles
4. Cross Wind Interference 5. Impulsive Loadings

I. Johnston, G. W., Seshagiri, B. V., Ellis, N. D. II. UTIAS Report No. 185

A two-dimensional, incompressible, potential flow solution based on A.M.O. Smith's method has been developed capable of predicting the unsteady interference pressure loadings on either moving or stationary bodies of arbitrary shape due to the passage of a second body. The pressure distribution has been suitably integrated to yield overall forces (side and axial) and moments (rolling and yawing). Effects of crosswinds of arbitrary magnitude and direction can be accurately included. The results of a wide range of computations using different body configurations are presented and analysed. The studies carried out indicate that substantial aerodynamic interference loads may be expected under real train passage conditions. These loads, impulsive in nature, depend on the type of body geometry, the lateral spacing between the bodies, and the closing velocity. In general, streamlining greatly reduces these loads, as does increased lateral spacing. Crosswinds significantly alter the predicted loadings, tending to increase them. The interference loading induced on a stationary vehicle when passed by a moving vehicle appears to impose the most critical design loads, for conditions of zero crosswind. Velocity scaling of the interference loadings presents inherent difficulties due to the basic unsteady nature of the problem. No simple and generally applicable velocity scaling laws are expected to emerge for this problem, however over limited ranges of conditions "ad hoc" velocity rules (trends) can certainly be obtained. The basic unsteady nature of this problem also greatly complicates experimental studies. The usual steady state wind tunnel methods will generally be inadequate; preference is strongly indicated for true unsteady motion simulation at reduced physical scale.

Available copies of this report are limited. Return this card to UTIAS, if you require a copy.

UTIAS Report No. 185

Institute for Aerospace Studies, University of Toronto

AERODYNAMIC INTERFERENCE OF HIGH SPEED GROUND VEHICLES

Johnston, G. W., Seshagiri, B. V., Ellis, N. D. 34 pages 26 figures 5 tables

1. Aerodynamic Interference 2. Unsteady Potential Flow 3. Ground Vehicles
4. Cross Wind Interference 5. Impulsive Loadings

I. Johnston, G. W., Seshagiri, B. V., Ellis, N. D. II. UTIAS Report No. 185

A two-dimensional, incompressible, potential flow solution based on A.M.O. Smith's method has been developed capable of predicting the unsteady interference pressure loadings on either moving or stationary bodies of arbitrary shape due to the passage of a second body. The pressure distribution has been suitably integrated to yield overall forces (side and axial) and moments (rolling and yawing). Effects of crosswinds of arbitrary magnitude and direction can be accurately included. The results of a wide range of computations using different body configurations are presented and analysed. The studies carried out indicate that substantial aerodynamic interference loads may be expected under real train passage conditions. These loads, impulsive in nature, depend on the type of body geometry, the lateral spacing between the bodies, and the closing velocity. In general, streamlining greatly reduces these loads, as does increased lateral spacing. Crosswinds significantly alter the predicted loadings, tending to increase them. The interference loading induced on a stationary vehicle when passed by a moving vehicle appears to impose the most critical design loads, for conditions of zero crosswind. Velocity scaling of the interference loadings presents inherent difficulties due to the basic unsteady nature of the problem. No simple and generally applicable velocity scaling laws are expected to emerge for this problem, however over limited ranges of conditions "ad hoc" velocity rules (trends) can certainly be obtained. The basic unsteady nature of this problem also greatly complicates experimental studies. The usual steady state wind tunnel methods will generally be inadequate; preference is strongly indicated for true unsteady motion simulation at reduced physical scale.

Available copies of this report are limited. Return this card to UTIAS, if you require a copy.

UTIAS Report No. 185

Institute for Aerospace Studies, University of Toronto

AERODYNAMIC INTERFERENCE OF HIGH SPEED GROUND VEHICLES

Johnston, G. W., Seshagiri, B. V., Ellis, N. D. 34 pages 26 figures 5 tables

1. Aerodynamic Interference 2. Unsteady Potential Flow 3. Ground Vehicles
4. Cross Wind Interference 5. Impulsive Loadings

I. Johnston, G. W., Seshagiri, B. V., Ellis, N. D. II. UTIAS Report No. 185

A two-dimensional, incompressible, potential flow solution based on A.M.O. Smith's method has been developed capable of predicting the unsteady interference pressure loadings on either moving or stationary bodies of arbitrary shape due to the passage of a second body. The pressure distribution has been suitably integrated to yield overall forces (side and axial) and moments (rolling and yawing). Effects of crosswinds of arbitrary magnitude and direction can be accurately included. The results of a wide range of computations using different body configurations are presented and analysed. The studies carried out indicate that substantial aerodynamic interference loads may be expected under real train passage conditions. These loads, impulsive in nature, depend on the type of body geometry, the lateral spacing between the bodies, and the closing velocity. In general, streamlining greatly reduces these loads, as does increased lateral spacing. Crosswinds significantly alter the predicted loadings, tending to increase them. The interference loading induced on a stationary vehicle when passed by a moving vehicle appears to impose the most critical design loads, for conditions of zero crosswind. Velocity scaling of the interference loadings presents inherent difficulties due to the basic unsteady nature of the problem. No simple and generally applicable velocity scaling laws are expected to emerge for this problem, however over limited ranges of conditions "ad hoc" velocity rules (trends) can certainly be obtained. The basic unsteady nature of this problem also greatly complicates experimental studies. The usual steady state wind tunnel methods will generally be inadequate; preference is strongly indicated for true unsteady motion simulation at reduced physical scale.

Available copies of this report are limited. Return this card to UTIAS, if you require a copy.